March 1967

Report No. 4848-2

conesco

consultants in

engineering science

a division of flow corporation

Final Report

THE PREPARATION OF SIMPLIFIED MANUALS FOR SHIELDING ANALYSIS

Supplement One: "In and Down" Scattering
and
Finite Fields of Contamination

by

Albert W. Starbird
John F. Batter

Prepared for

Office of Civil Defense
Office of the Secretary of the Army
Washington, D. C.

Under Contract OCD PS 65-67

127 coolidge hill road • watertown, massachusetts 02172

CONESCO consultants in engineering science

March 1967 4848-2

Final Report

THE PREPARATION OF SIMPLIFIED MANUALS FOR SHIELDING ANALYSIS

Supplement One: "In and Down" Scattering and Finite Fields of Contamination

by

Albert W. Starbird
John F. Batter

OCD Review Notice

This report has been reviewed in the Office of Civil Defense and approved for publication. Approval does not signify that the contents necessarily reflect the views and policies of the Office of Civil Defense

Prepared for

Office of Civil Defense
Office of the Secretary of the Army
Washington, D. C.

Under Contract OCD PS 65-67

SUMMARY

A study was undertaken to examine present and proposed methods of calculating the attenuation afforded "in and down" scattered radiation by a horizontal slab, and the effects of finite fields of contamination in order to recommend improvements and up dating for OCD documents TR-20, Volumes 1 and 2, "Shelter Design and Analysis."

In this study we examined the assumption used in computing the "in and down" attenuation factor, assessed their effect on the resulting attenuation factors, and compared the results with the latest available experimental data. Recommendations are provided as to "best value" factors and how they might be included in existing publications.

The effects of finite fields of contamination were subjected to further analysis by directly comparing the existing method of calculation with results obtained using transmission coefficients calculated by the Monte Carlo method. This comparison, though complete only for above-ground locations, indicates that further study is required before the existing method of calculation can be relied upon.

The study of in and down scattered radiation is described in Chapters 1 through 3; finite fields of contamination are in Chapter 4. These major conclusions may be drawn from this study:

The "In and Down" Attenuation Factor

1. The in and down attenuation factor, $(B'_o(X, \bar{\omega})$, represents a significantly better estimate of this effect than the values previously used $(B'_o(X))$.

2. Calculated and measured attenuation factors agree within 18.5 per cent; the analytical value is conservative. It was found that the standard deviation of the ratio of the attenuation calculated, $B'_o(X,\bar{\omega})$, to that measured in 346 experimental measurements, was 13.5 per cent.

Finite Fields of Contamination

3. The current method of computing the effects of finite fields of contamination requires further study.

4. In total dose, the NBS Monte Carlo compilation method[20] and that presently proposed [9] agree fairly well for detector locations on the first floor of a sheltering structure.

5. Major differences in the fraction of scatter to direct dose were found when using the NBS method, casting serious doubt on the accuracy of current methods of shelter analysis when the detector is shielded from direct radiation (i.e., in a basement or an upper-story location shadowed by a heavy floor).

TABLE OF CONTENTS

LIST OF ILLUSTRATIONS

List of Illustrations (Cont'd)

LIST OF TABLES

CHAPTER 1

IN AND DOWN SCATTERED RADIATION – THEORY

INTRODUCTION

Most of the error observed between measured and computed values of dose rate in basement areas has been attributed to the attenuation provided by the basement ceiling. Values of this attenuation previously were computed in approximate form for cobalt, cesium, and the 1.12 hr. fallout energy spectrum, using a single Compton scatter energy change and transmission coefficients computed by the Monte Carlo method, assuming that all incident radiation lay in the plane mutually perpendicular to the exterior wall and the ground and that it passed through the detector location. Agreement between the attenuation computed in this approximate fashion and that measured was much better than that obtained with the engineering method.

Our purpose in this study has been to re-examine the effects of the assumptions used and to recalculate the basement ceiling attenuation more accurately by (1) relaxing the restriction that incident radiation must lie in the plane containing the detector that is mutually perpendicular to the ground and the wall and (2) using a finer gradient when performing the numerical integration over the contaminated area.

Basement Ceiling Attenuation

Approximately 80 per cent of the radiation arriving at the exterior wall of a structure located in an infinite contaminated field is uncollided. The remaining 20 per cent is singly or multiple scattered radiation of lower energy. This "atmospheric" scattered radiation is divided about evenly between the upper and lower hemisphere for a detector located above ground level. Thus, in estimating the attenuation afforded by a basement ceiling, the first assumption is that all radiation arriving at the above-ground walls of a structure that scatters to the basement area is uncollided. According to this assumption, all scattered radiation is of higher energy, therefore attenuating less rapidly than actual scattered radiation, hence producing a conservative estimate of the radiation scattered to a below-ground area. To simplify the problem, we adopted a second assumption: radiation scattered by the above-ground portion of the structure is reduced in energy by a single Compton scatter, through the angle required to reach the detector only. This assumption is also conservative in that it treats all multiply scattered photons as of higher than their actual energy. Raso has computed the average energy of scattered photons for incident energy of 1.25 mev and finds that this figure is about 85 per cent of that predicted by single-scatter theory. The third major assumption is that the detector is relatively near the basement

ceiling; i.e., radiation arriving at a basement detector by a ceiling slab is attenuated exactly as much as that of parallel monoenergetic radiation of the same energy and angular incidence in relation to the external surface of the basement ceiling.

The procedure used to compute the ceiling attenuation was as follows (see Figure 1). The contaminated field was subdivided into "n" increments of equal radiation worth, for each of the nine energy components of the 1.12 hr. fallout spectrum, when viewed by a detector located at the scattering area. The total angle of scatter (ψ) then was determined at the scattering location between the source patch and the detector. Notice that the previously used model for computation was a cylinder (or the equivalent, the short wall of a building with large eccentricity) and therefore the exit azimuthal angle β was identically zero. Then, the new scattered energy was computed from the Compton scatter equations. The dose arriving at the detector location is taken as proportional to the amount of radiation energy arriving at the wall from the source patch, reduced by the ratio of the initial energy to that found after scattering, and multiplied by the attenuation introduced by the basement ceiling (taken as equal to that of parallel monoenergetic radiation of identical energy and angular incidence) and the air absorption coefficient. A quantity proportional to the total overall dose may then be calculated by summing this quantity over all energies of the fallout spectrum weighed by the energy spectrum and over the infinite plane contaminated area. The ceiling attenuation factor was then computed by dividing this quantity by the similar quantity for zero ceiling thickness.

This may be expressed in equations in the form presented here (see Figure 1). The contaminated field beyond the wall is subdivided into a total of "n" contaminated patches of equal worth (when viewed by a detector located at the wall scattering volume) in cylindrical geometry. The total uncollided dose rate at height h from a semi-infinite field of contamination is:

$$D(E) = \text{const} \int_{\mu h}^{\infty} \frac{e^{-\mu_t(E)\rho} 2\pi\rho d\rho}{\rho^2} = \text{const}\, E_1(\mu(E)h)$$

where:

$\mu_t(E)$ = is the total coefficient in air for photon energy E

h = the height of the scattering element

ρ = the slant distance from detector to differential source area

E_1 = the exponent integral of the first kind

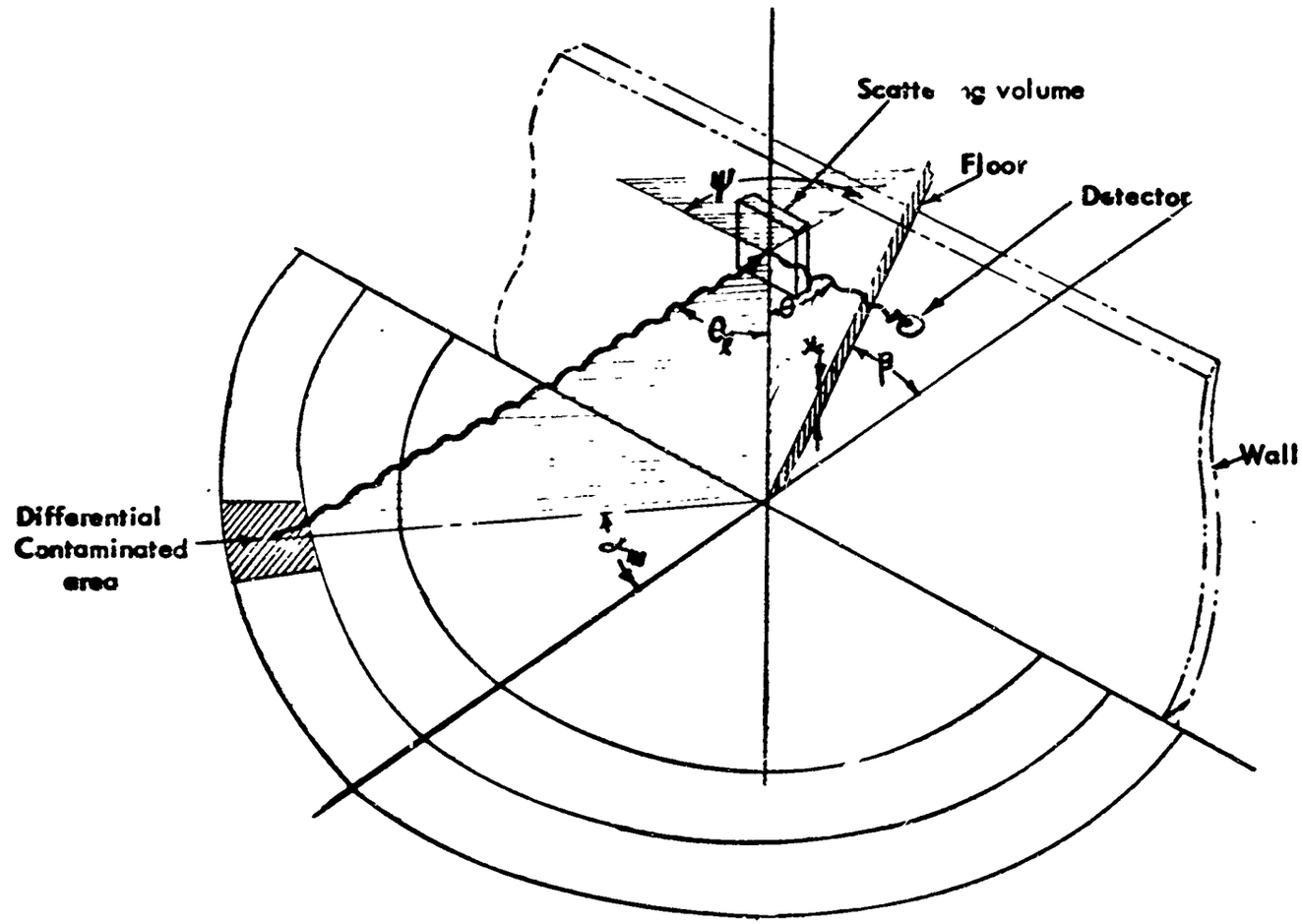

Figure 1

GEOMETRY FOR WALL-SCATTER CALCULATION

The total number of differential patches "n" is composed of "i" rings of equal worth, each subdivided into "j" azimuthal patches. The center of each patch thus is specified by coordinates θ_l and a_m relative to the scattering area.

a_m = the azimuthal coordinate (see Figure 1) of source patch "m"

$$a_m = \frac{\pi(m + 1/2)}{2_j}$$

$\theta_l(E)$ = the polar coordinate of a source patch for contamination of energy E

$$\theta_l(E) = \cos^{-1} \frac{\mu_t(E)h}{\mu_t(E)\rho_l}$$

$$E_1(\mu_t(E)\rho_i) = \frac{\left[E_1(\mu_t(E)h)\right] \quad (l + 1/2)}{i}$$

For heights of the scattering volume "h" that are small with respect to a mean free path, the quantity $\theta_i(E)$ is nearly independent of "h".

The detector is located with respect to the scattering volume by azimuthal angle β and polar angle θ. The cosine of the total angle through which a photon must scatter from the source patch "l", "m", to reach the detector therefore is:

$$\cos\psi = \left\{\cos\theta \cos\theta_l - \sin\theta \sin\theta_l \cos(180 - a_m - \beta)\right\}$$

which is implicitly a function of the initial energy E_o. Thus the energy E in mev of the radiation scattered by the wall toward the detector, after suffering a single Compton scatter, would be

$$E = E_o \left\{\frac{.51}{.51 + E_o(1 - \cos\psi)}\right\}$$

If the probability that a photon will scatter from source patch θ_1, α_m to a detector located at θ, β relative to the scattering volume, is written as $P(\theta_1, \alpha_m \rightarrow \theta, \beta)$, the dose seen by such a detector located below a floor of thickness X from a single Compton scatter is

$$D(E_o, X, \theta, \beta) = \frac{\Delta E_o P(\theta_1, \alpha_m \rightarrow \theta, \beta) E \mu_a(E) \cos\theta S'(X, \cos\theta, E)}{n \qquad E_o}$$

where:

ΔE_o = the total quantity of energy E_o incident on the scattering volume

E_o = the energy of interest

E = the energy of the photon after suffering a single scatter to the detector

$\mu_a(E)$ = tissue equivalent energy absorption cross section

$\cos\theta S'(X, \cos\theta, \omega E)$ = attenuation factor for parallel monoenergetic radiation of energy E, angle of incidence θ, and slab thickness X

The attenuation introduced by the ceiling above the detector therefore is equal to the integral of this quantity over the total scattering volume (the wall) divided by the same quantity, with thickness X equal to zero. In practice the quantity $P(\theta_1, \alpha_m \rightarrow \theta, \beta)$ is nearly constant and may be removed from under the integral sign and canceled. If $P(\theta_1, \alpha_m \rightarrow \theta, \beta)$ is taken as approximately equal to the differential Compton scatter term rather than constant, the differences are quite small. This is illustrated in Table 1 for the region of most interest, cos θ. Here agreement is found to be well within the region of other uncertainties of the calculation.

TABLE 1

Comparison of attenuation factors computed with probability of scatter equal to the Compton differential scatter probability and a constant for $\beta = 0$ and $E_o = 1.25$ mev

cos θ	1.0		.75		.50		.25		.10	
Scatter probability	Comp.	Const.	Comp.	Const.	Comp.	Const.	Comp.	Const.	Comp.	Const.
X_f										
10 psf	.90	.89	.83	.82	.68	.67.	.39	.36	.13	.12
20 psf	.76	.72	.64	.62	.45	.42	.18	.16	.035	.032
40 psf	.49	.43	.37	.38	.19	.18	.052	.050	.010	.0091
80 psf	.18	.12	.11	.029	.039	.038	.0086	.0070	.0018	.0016
160 psf	.023	.010	.0098	.0068	.018	.0014	.0038	.00030	.00081	.00061

For simplicity, the scattering probability may therefore be taken as constant over the range of interest of this problem, and the attenuation at position θ, β may be written as

$$\mathrm{Att}(\theta, \mu, X, E_o) = \frac{\sum_{ij} \frac{E}{E_o} \mu_a(E) \cos\theta S'(X, \cos\theta, E)}{\sum_{ij} \frac{E}{E_o} \mu_a(E) \cos\theta S'(X = 0, \cos\theta, E)}$$

Two aspects of the problem may now be evaluated quite easily. First, since Raso[2] found that the average energy of scattered photons was about 85 per cent of Compton single-scatter energy, what effect would this degradation of energy of the scattered photons have? Second, what effect other than the straightforward

geometric difference of slant penetration distance in the floor would a variation in angle beta have on the attenuation factor?

These effects are illustrated in Table 2. Here again it is evident that essentially there is no secondary geometric effect on the floor attenuation and that the assumption of scattered energy equal to 85 per cent of Compton single scatter lowers the attenuation factors by only a small amount.

Since most buildings are other than cylindrical in shape the necessary integration over the variable beta must be examined. Previously, it was assumed that the angular distribution of radiation emerging from the rear of a vertical wall in the plane parallel to the ground is closely approximated by the cosine of the emergent angle relative to a perpendicular to the scattering surface. It was demonstrated above (see Table 2) that the principal effect of this angle being other than zero is in the straightforward geometric increase in the slant penetration distance of the slab over the detector that a photon must traverse to reach a detector a given distance from the wall. This distance, represented equivalently by an increase in the angle θ to θ' for an attenuating slab of constant thickness, may be calculated quickly by the relationship:

$$\text{Tan } \theta' = \tan \theta / \cos \beta$$

The attenuation afforded by a rectangular structure may, then, be calculated in a manner similar to that applied to a cylindrical structure by integrating the dose scattered from a given scattering volume (represented by angle β), weighed by the emergent angular distribution for a finite thickness slab divided by the similar quantity for a slab of zero thickness. Thus

$$B'_o\left(X, \theta, E_o, \frac{L}{W}\right) = \frac{\int_{\text{all walls}} \Delta D\,(\theta', \beta, X, E_o) \cos \beta \, d\beta}{\int_{\text{all walls}} \Delta D\,(\theta', \beta, X = 0, E_o) \cos \beta \, d\beta}$$

where $B'_o(X, \theta, E_o, \frac{L}{W})$ = the attenuation that would be afforded by a slab to in and down scattered radiation in a rectangular structure.

TABLE 2

Comparison of Attenuation Factors for Various Emergent Angles Beta and Various Assumptions as to Scattered Energy

cos θ	1.0			.75			.50			.25			.10		
Beta	60°	0°	0°	60°	0°	0°	60°	0°	0°	60°	0°	0°	60°	0°	0°
Scat. energy / Single scat. energy	1.0	1.0	.85	1.0	1.0	.85	1.0	1.0	.85	1.0	1.0	.85	1.0	1.0	.85
Thickness															
10 psf	.89	.89	.89	.78	.82	.8'	.65	.67	.65	.33	.36	.33	.11	.12	.11
20 psf	72	.72	.71	.58	.62	.60	.40	.42	.40	.14	.16	.14	.030	.032	.029
40 psf	.43	.43	.41	.35	.33	.35	.17	.18	.16	.043	.044	.040	.0087	.0091	.0083
80 psf	12	.12	.11	.080	.0 2	.076	.029	033	.028	.0066	.0070	.0061	.0014	.0015	.0014
160 psf	.0098	.010	.0054	.0058	.0068	.0046	.0013	.0014	.0011	.00028	.00030	.00026	.000058	.000061	.000050

L/W = length-to-width ratio of the structure

This quantity has been calculated for several conditions of floor mass, building size, and eccentricity by numerically summing over the azimuthal distribution in 5^{o} increments. The results of this series of computations are shown in Table 3, where they are compared with the values obtained by computing the floor attenuation of a cylindrical structure of equal solid angle fraction when

TABLE 3

Comparison of attenuation factors computed in circular and rectangular geometry for equal solid angle fraction, $\bar{\omega}$
E = 1.25 mev

(Note Structure is of differential wall height)

Solid angle fraction	Floor thickness (psf)	Rectangular		Circular
		Eccentricity	Att.	Att.
0.29	10	1.00	.80	.80
0.39	10	.51	.77	.74
0.44	10	.23	.65	.70
0.54	10	1.00	.56	.58
0.63	10	.45	.43	.46
0.78	10	1.00	.26	.28
0.29	80	1.00	.081	.080
0.39	80	.51	.057	.057
0.44	80	.23	.052	.048
0.54	80	1.00	.027	.027
0.63	80	.45	.018	.017
0.78	80	1.00	.0057	.0058

viewed by the detector. This table indicates that these two methods give excellent agreement and that there is therefore no significant "geometry factor" for floor attenuation.

The assumptions made in calculating the attenuation afforded to in and down scattered radiation by a floor slab upon evaluation, have been found to effect but little the predicted attenuation values. Using a constant-scatter probability

rather than the Compton single-scatter probability slightly decreases the predicted basement detector dose rates, whereas assuming scatter energy equal to the single Compton scatter energy and neglecting secondary geometric effects in the rectangular wall case slightly increases predicted dose rate.

The floor barrier computation as described above has been performed for the approximate energy of cesium and cobalt radiation as well as for each of the nine energy components of the 1.12 hr. fallout spectrum. Figures 2 through 4 present the results of this series of computations as a function of the mass thickness of the attenuating slab and the solid angle to the scattering volume. In Figure 4 is presented the result of summing the data for the nine energy groups of the 1.12 hr. fallout spectrum weighed by the value of each of these groups. Previously estimated values produced by a rough hand calculation are generally within about 10 per cent of the values shown.

The use of these figures is quite straightforward. In calculating the exact dose in the basement area, the dose from each differential increment of height of the scattering wall should be multiplied by the attenuation factor (Figures 2 through 4) for the basement ceiling at the solid angle fraction of that differential wall height (when viewed by the detector) and these results summed over the entire scattering wall height. It was demonstrated earlier, however,[1] that an equivalent value, generally within 10 per cent of that calculated by this method, may be obtained easily by averaging the solid angle to the top and bottom of the scattering wall and determining the attenuation factor for this average solid angle fraction. Several examples of this procedure (for a structure of 10 ft. wall height with a detector 7 ft. below the floor) are:

Building plan area	Wall thickness	$B_o(\bar{\omega},X)$*	$\int_o^h B_o(\omega,X)dh$*
20 x 20	25	0.45	0.48
	50	0.19	0.20
40 x 40	25	0.26	0.28
	50	0.086	0.098
100 x 100	25	0.080	0.083
	50	0.018	0.019

*More properly, these quantities should be $B_o(\bar{\omega},X)L(d)$ and $\int_o^h B_o(\omega,X)L(d)dh$, where L(d) represents the dose variation with height d above the contaminated plane. If this further refinement is included, both quantities are reduced slightly, the integral quantity always being reduced more than the multiplication quantity. If the scattering wall extends from zero to 10 ft., the integral quantity is reduced by approximately 8 per cent, while $B_o(\bar{\omega}, X)L(d)$ remains essentially the same.

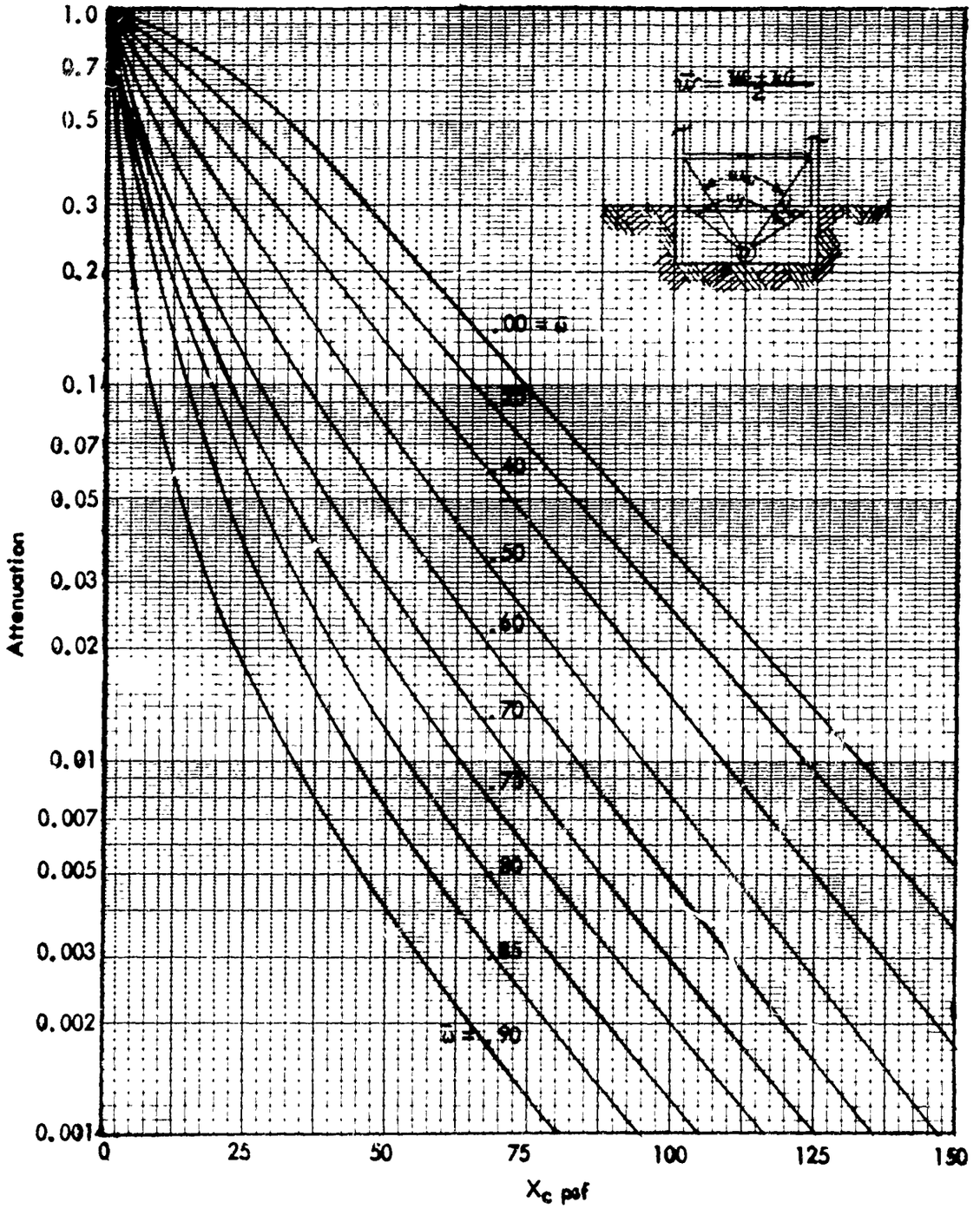

Figure 2

FLOOR ATTENUATION, 0.67 mev

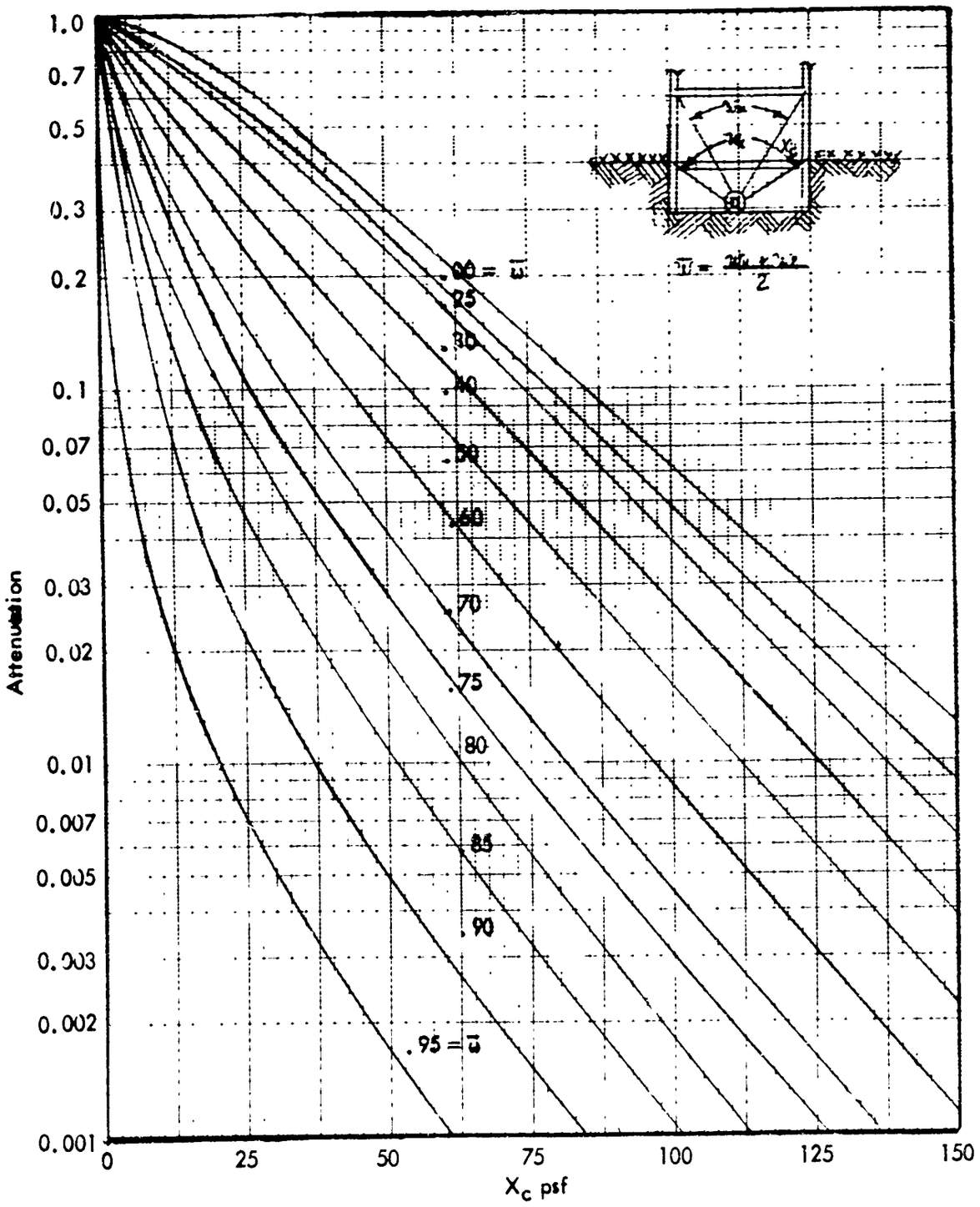

Figure 3

FLOOR ATTENUATION, 1.25 mev

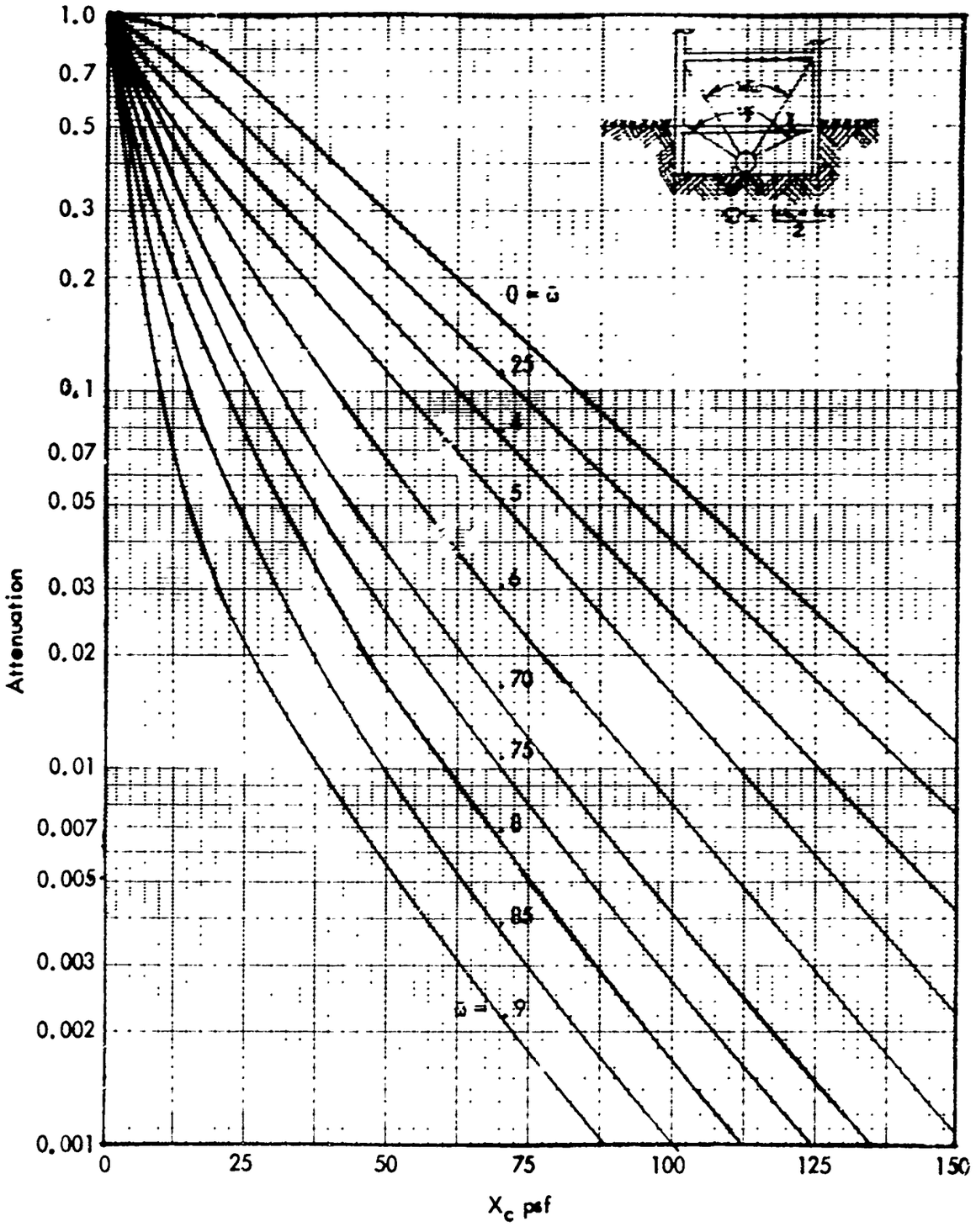

Figure 4

FLOOR ATTENUATION, 1.12 hr fallout

CHAPTER 2

IN AND DOWN SCATTERED RADIATION — EXPERIMENT

INTRODUCTION

Over the past few years several experiments have provided data useful in verifying the basement ceiling barrier factor, $B'_o(X_f,\bar{\omega})$, developed in this report.[5] Recent experiments at the Defense Chemical, Biological and Radiation Laboratories in Canada, at the Protective Structures Development Center,[6] and at Technical Operations Research,[7,8] were performed in such a way as to determine $B'_o(X_f,\bar{\omega})$ by comparing measured results with and without a basement ceiling slab in position. In addition, several other total building experiments have been performed that are useful in comparing measured and computed basement data. The latter experiments either were not specifically designed for "in and down" measurements or the only results available to date are of a preliminary nature limiting their comparison to the total basement protection factor, without isolating the ceiling barrier factor component, $B'_o(X_f,\bar{\omega})$. Brief comparisons are here presented, however, between building attenuation values computed by means of the new barrier curves $B'_o(X_f,\bar{\omega})$ of this report and the measured results. Of the work cited, only the DCBRL experiment is covered in detail in this report. The remaining experiments have been covered in the Conesco report entitled "The Preparation of Simplified Manuals for Shielding Analysis."[1]

"In and Down" Scattering Measurements at the Defense Chemical, Biological and Radiation Laboratories"[5]

The experimental arrangement (see Figure 5) for the "In and Down" scattering study at DCBRL[5] consisted of measuring the dose distributions produced by the radiation transmitted and scattered from a vertical barrier that penetrated an adjacent horizontal barrier. A Cesium-137 source collimated to a 10° half angle by a lead-filled collimator was utilized as the radiation source. This radiation beam impinged on a 3 ft. high by 4 ft. long vertical concrete slab, providing an effective circular pattern of incident dose spread over an area 20.5 in. in radius. This area was centered at the physical center of the slab on the slab face. Measurements of the scattered dose were taken along a vertical traverse positioned 12, 24, and 36 inches to the rear of the vertical slab at depths below the top surface of the horizontal slab ranging from 3-3/4 to 30 in. Vertical slab thickness variations were 0 psf, 6.45 psf plywood, and 34 and 68 psf concrete. The horizontal slabs were of 0, 36.5, and 73 psf of reinforced concrete. The detectors were partially shielded with lead to limit their exposure to multiple scattering from the ground.

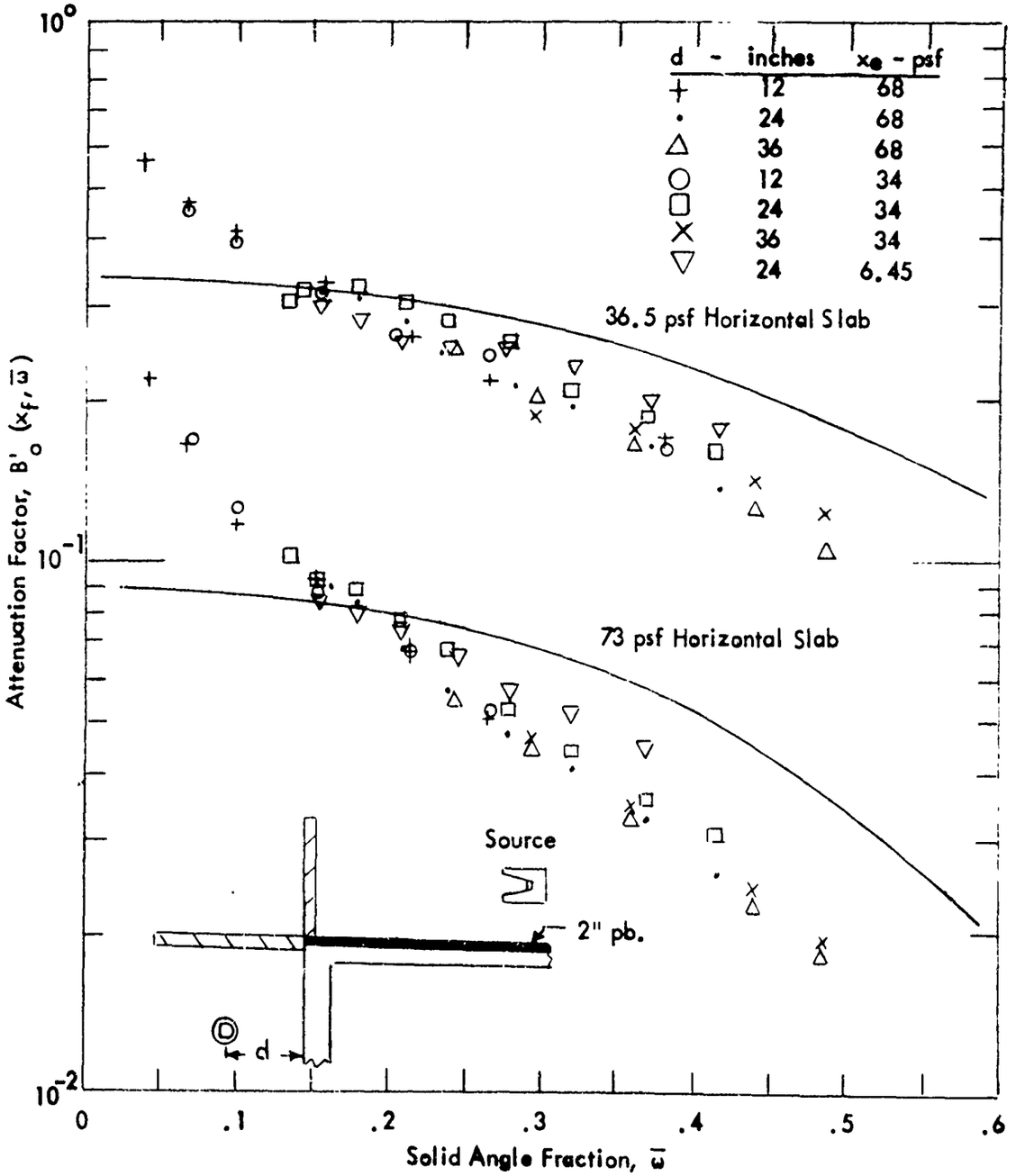

Comparisen of Theory With DCBRL Measurements[5]
Cesium - Concrete

Figure 5

The attenuation attributed to the horizontal (ceiling) barrier was determined by taking the ratio of the scattered radiation dose values with the horizontal barrier in position to the respective measured values for the zero psf horizontal barrier case. Measured attenuation values versus average solid angle fraction, $\bar{\omega}$, are shown in Figure 5. This average solid angle fraction, $\bar{\omega}$, for the vertical wall subjected to the 20.5 in. radius incident beam was approximately determined from ω_l and ω_u values based on the lower and upper limits of an equivalent square area (36 by 36 in.) of incident radiation. Figure 5 also presents the theoretical attenuation curves for 36.5 and 75 psf ceilings, as calculated by the method used in this report for cesium (.66 mev) radiation impinging perpendicularly on the vertical slab. The majority of the experimental points fall below the theoretical curves except at small values ($\bar{\omega} \leq .175$) of $\bar{\omega}$, where experimental dose rates were higher than those predicted by theory. This increase above the theoretical curves at small $\bar{\omega}$ is not expected and cannot be explained at this time. The values of dose upon which these data at small $\bar{\omega}$ are based are extremely low and any unaccounted air-scattered or ground-penetration components even in small quantities could contribute significantly at these low rate regions, providing a false reading of this type. Results of other experiments discussed later in this chapter did not show this crossover at small values of $\bar{\omega}$.

"In and Down" Measurements at the Protection Structures Development Center[6]

Cobalt-60 measurements were performed on a 24 by 36 ft. rectangular concrete structure with a basement having an exterior-wall thickness of 50 psf. The experiment was conducted both with and without a 50 psf concrete basement ceiling slab, so that the basement ceiling effect could be measured directly. In Figure 6 is presented the comparison between the measured ceiling effect, $B'_o(X_f,\bar{\omega})$ and that taken from the theoretical values of this report as given in Figure 3. The 50 psf theoretical curve falls slightly above the 50 psf measured values, giving a ratio of experiment to theory of approximately 0.76. The computed values in this case therefore were both conservative and close to the 0.815 mean experiment to theory ratio determined for all the experiments covered in this report. (See concluding section of this chapter.)

Attenuation of Cobalt-60 Radiation by a Small Iron Cylindrical Structure[7,8]

A series of measurements were conducted on a 2 ft. diameter cylindrical iron structure. The structure was composed essentially of an iron pipe 2 ft. in diameter mounted vertically in the ground so that only the upper 2 ft. of its length projected above the ground level. The above-ground wall thickness of this structure was varied from 1/4 to 1-1/2 in. (approximately 5-60 psf) with floor thicknesses of 0, 10, 20, and 40 psf iron. Below-ground, i.e., basement measurements were made

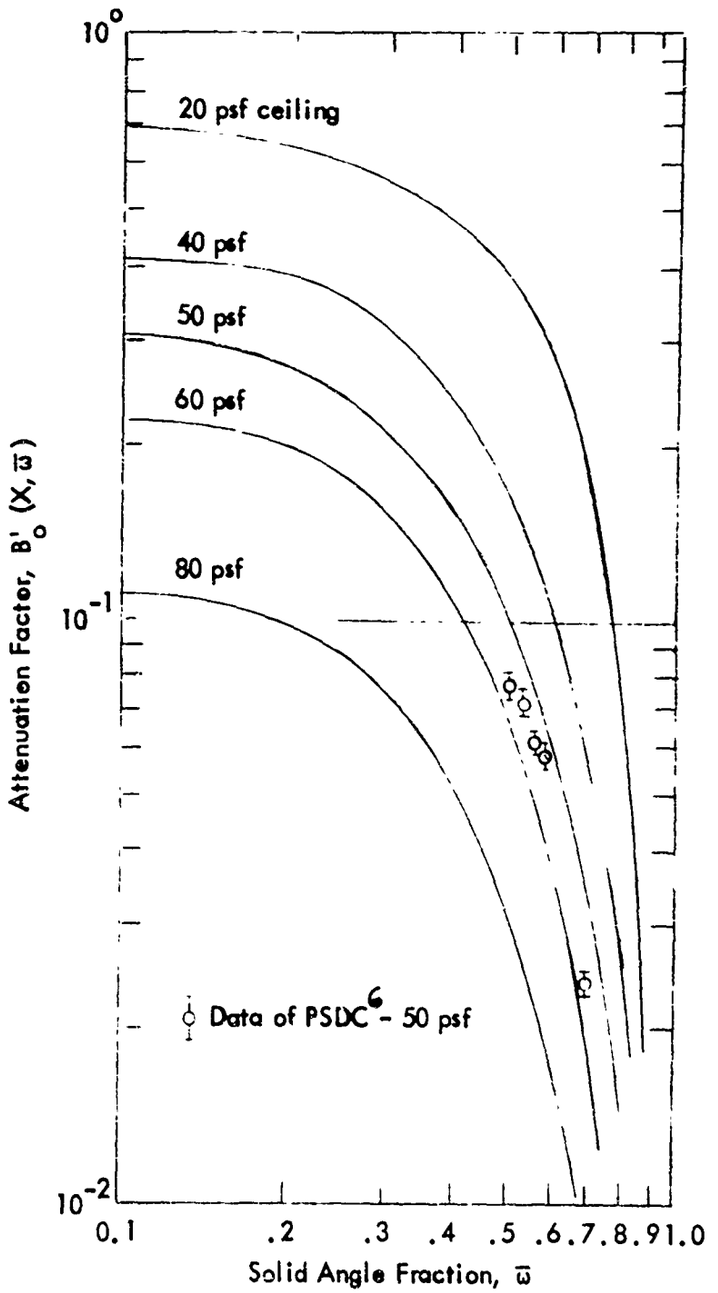

Basement Ceiling Attenuation
Cobalt - Concrete

Figure 6

along the vertical centerline at depths of 1/4, 1/2, 3/4, 1, 2, and 3 ft. Results expressed as the ratio of the measured dose rate in the basement with the ceiling in place to that measured without the ceiling (zero psf), a direct measure of attenuation factor $B'_o(X_f,\bar{\omega})$, are presented in Figure 7.

The measured floor reduction factors vary with solid angle fraction in a manner similar to that of the theoretical curves based on the theory developed in this report. The measured values are somewhat lower (more conservative) than predicted by theory, as would be expected, since all assumptions and approximations used in developing the theory were aimed at producing a conservative attenuation value.

Basement Attenuation — Other Experiments

A comparison of experimentally measured dose rates with those computed by the Engineering Manual[9] method (modified for Cobalt-60 concrete), using both the floor attenuation data given in that report and those provided by the method developed in this report, is presented in Table 4 for all currently reported experiments. In general, agreement between experimentally measured values and the treatment recommended by this study is much better than that provided by the method currently used. In particular, the basement ceiling barrier experiments currently being made at NDL[10] (on a 10 by 20 ft. roofless concrete structure with 46 psf exterior walls and floor slab), though still preliminary, provide much better agreement with the method used in this report than Engineering Manual values, particularly at the lower depths. The same trend holds true for the data in an older study[11] of a simple structure with a basement, even though those data are somewhat difficult to interpret because of inhomogeneity in floor mass. The mean ratio of the experimental results of these two full-scale studies to those using the computed method of this report is approximately 0.70, compared to a mean of 0.815 for all experiments reported. Values calculated by the method used in this report are conservative compared with those provided by experiment and follow the dose versus depth contours better than previous analyses.

Protection factor versus depth contour agreement is also good for the Kansas State University[12] blockhouse and the Technical Operations multistory 1/12 scale steel models.[13,14] The KSU structure was a square 20 by 20 ft. concrete house of 60 psf walls and 56 psf floor and roof; the T/O model was of a 36 by 48 ft. six-story windowless building. The absolute measured level of the dose in the basement of the KSU blockhouse is higher (prediction less protection) than that computed by the method of this report -the only time that this has occurred in a full-scale structure. Dose rates in the basement of the 80 psf wall and floor steel model (T/O) also were higher than predicted. Reported misalignment of the structure with the basement and edge scattering of radiation from the relatively thick basement ceiling slab that projected above the ground level indicates, however, that the absolute value of the dose measured is of questionable validity in this case.

TABLE 4

Dose Rate in Below Ground Regions from Ground Based Sources of Contamination

	Depth, ft	Experiment	Engineering Manual	Method of This Report
NDL[10]	1	.0034	.0035	.0052
	2	.0033	.0023	.0054
	3	.0031	.0016	.0053
	4	.0029	.0010	.0043
	5	.0026	.00068	.0035
	6	.0024	.00048	.0028
Simple structure with basement[11]	1-3/4	.0019	.0010	.0025
	4-1/4	.0018	.00098	.0023
	6-3/4	.0017	.00101	.0026
	9-1/4	.0015	.00040	.0020
KSU blockhouse[12]	1/4	.0041	.0026	.0025
	1-3/4	.0048	.0018	.0025
	4-3/4	.0051	.00082	.0026
Multistory steel model[13, 14]				
20 psf walls	3	.0195	.0142	.0259
20 psf floors	10	.0185	.0055	.0185
	15	.0140	.0035	.0106
20 psf walls	1	.00094	.00164	.00101
80 psf floors	3	.00115	.00133	.00129
	7	.0016	.00075	.00143
	10	.0018	.00052	.00176
	15	.0018	.00034	.000127
80 psf walls	1	.00085	.00072	.00041
80 psf floors	3	.0030	.00058	.00051
	7	.0033	.00034	.00055
	10	.0034	.00023	.00070
	15	.0026	.00015	.00056
40 psf walls	3	.0022	.0034	.0040
50 psf floors	6	.0023	.0022	.0040
	9	.0021	.0017	.0048
	15	.0022	.00087	.0033

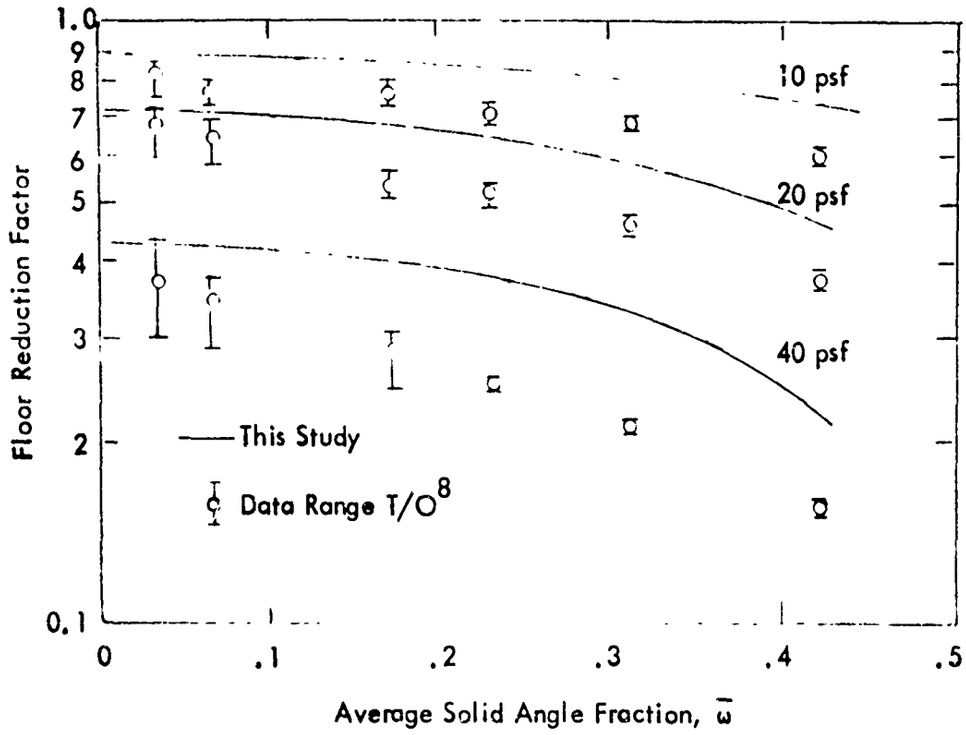

Floor Reduction Factor as Measured With a Steel Cylindrical Structure

Figure 7

Summary of Comparisons with Experiment

The method of this report for computing basement protection factors, using the value $B'_o(X_f,\bar{\omega})$ in determining the effect of the basement ceiling barrier, provides results that agree much better with measured basement attenuation than does the Engineering Manual method, particularly as detector depth below the ceiling slab increases. When comparing computed values based on the method used here with measured values, nearly all the computed values indicated slightly less attenuation than the comparable measured values. The computed or theoretical values therefore are conservative as compared with measured values.

Figure 8 illustrates the comparison between measured and computed values of $B'_o(X_f,\bar{\omega})$ of this report for the three experiments providing data for basement positions both with and without the ceiling slab in place (i.e., a direct measurement of barrier factor B'_o). All values fall on the conservative side of the figure except for a few of the DCBRL points taken at small solid angle fractions ($\bar{\omega} < .175$), where the effects of any radiation component not accounted for (skyshine is suspected) in these low dose rate areas would provide a significant part of the measured dose and would therefore seem to reflect a major decrease in the floor slab's effectiveness. Figure 9 shows the distribution of the ratios of all measured basement attenuation experimental values compared with that computed using the theory of this report. At ratios greater than 1.10, the tail on this graph can be attributed almost entirely to measurements at small solid angle fractions for the DCBRL experiment mentioned above, to the KSU data, and to the questionable 80 psf wall and floor T/O model multistory structure data. A statistical analysis of this distribution is shown in Figure 10, which clearly indicates the mean value of the experiment to computed dose ratio is 0.815 with a standard deviation, σ, of 0.135 for all the experimental data.

Since Figure 10 represents a sizable number of experimental data (approximately 350 experimental points), it is recommended that the mean ratio of experiment to theory of 0.815 be used to reduct the computed barrier function (Figures, 2, 3, and 4) of this report in order to provide better agreement. Clearly, it is not enough to multiply the computed values by this ratio, because the attenuation of a zero thickness floor must remain 1.0. In Figure 17 of Chapter 3, the floor barrier attenuation for the 1.12 hr. fallout spectrum has been corrected by multiplying by 0.815 for floor thickness greater than 20 psf, by .91 for floor thickness of 10 psf and faired into a value of 1.0 for floor thicknesses of zero psf. This chart thereby is brought into better agreement with expected experimental values. It is further recommended that a similar procedure be used for cobalt and cesium.

A report entitled "Dose Albedo and Transmission Coefficients for Cobalt-60 and Cesium-137 Gamma Rays Incident on Concrete Slabs"[15] by M. J. Berger and E. E. Morris was published when this report was nearing completion. The attenuation

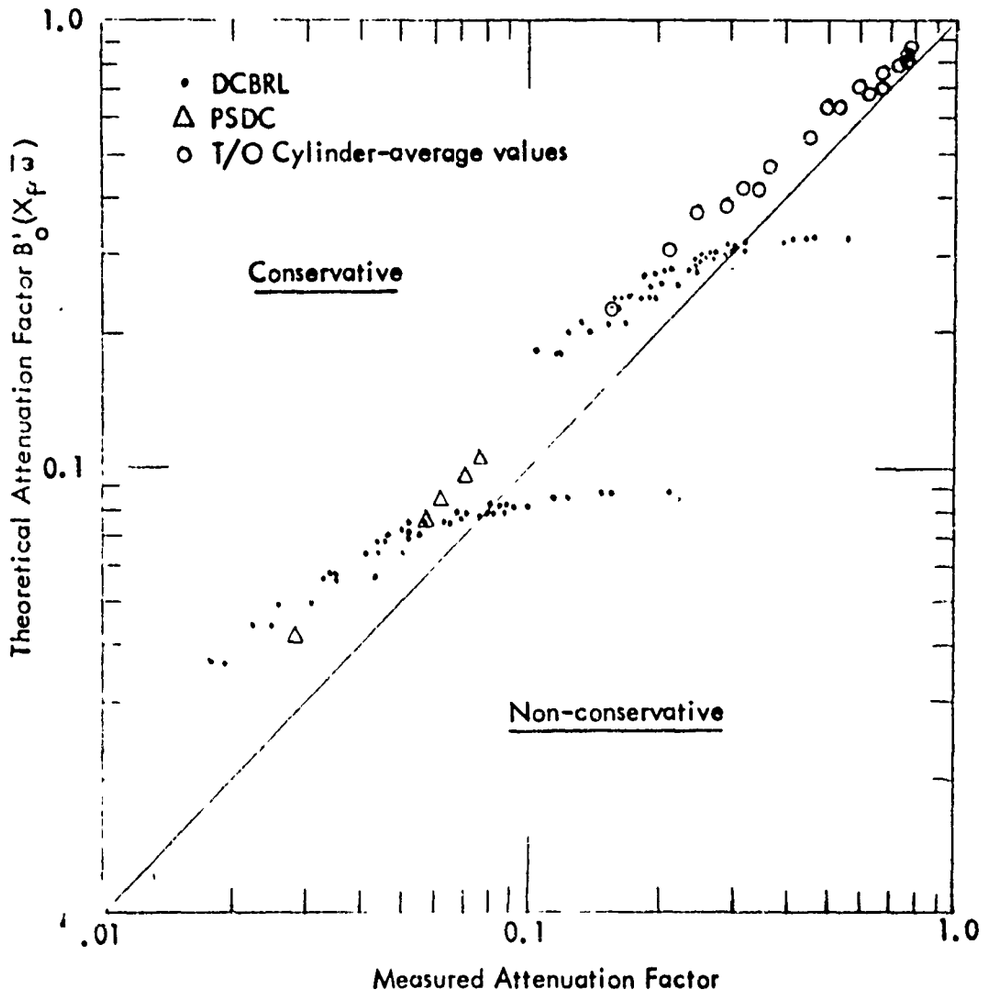

Theory Versus Experiment

Figure 8

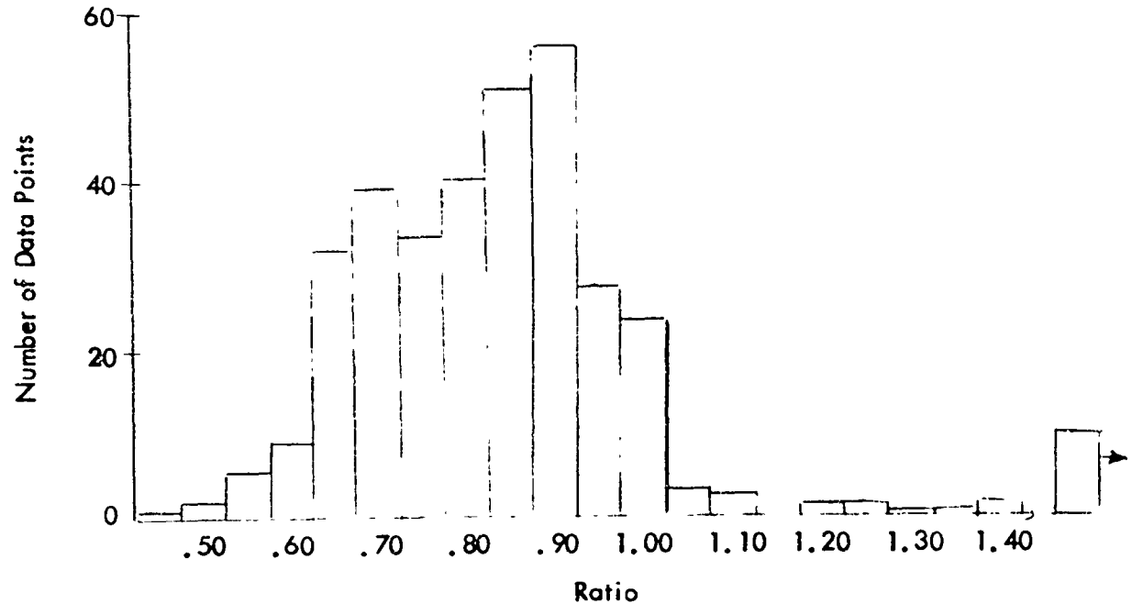

Distribution - Ratio of Measured Results to Theory

Figure 9

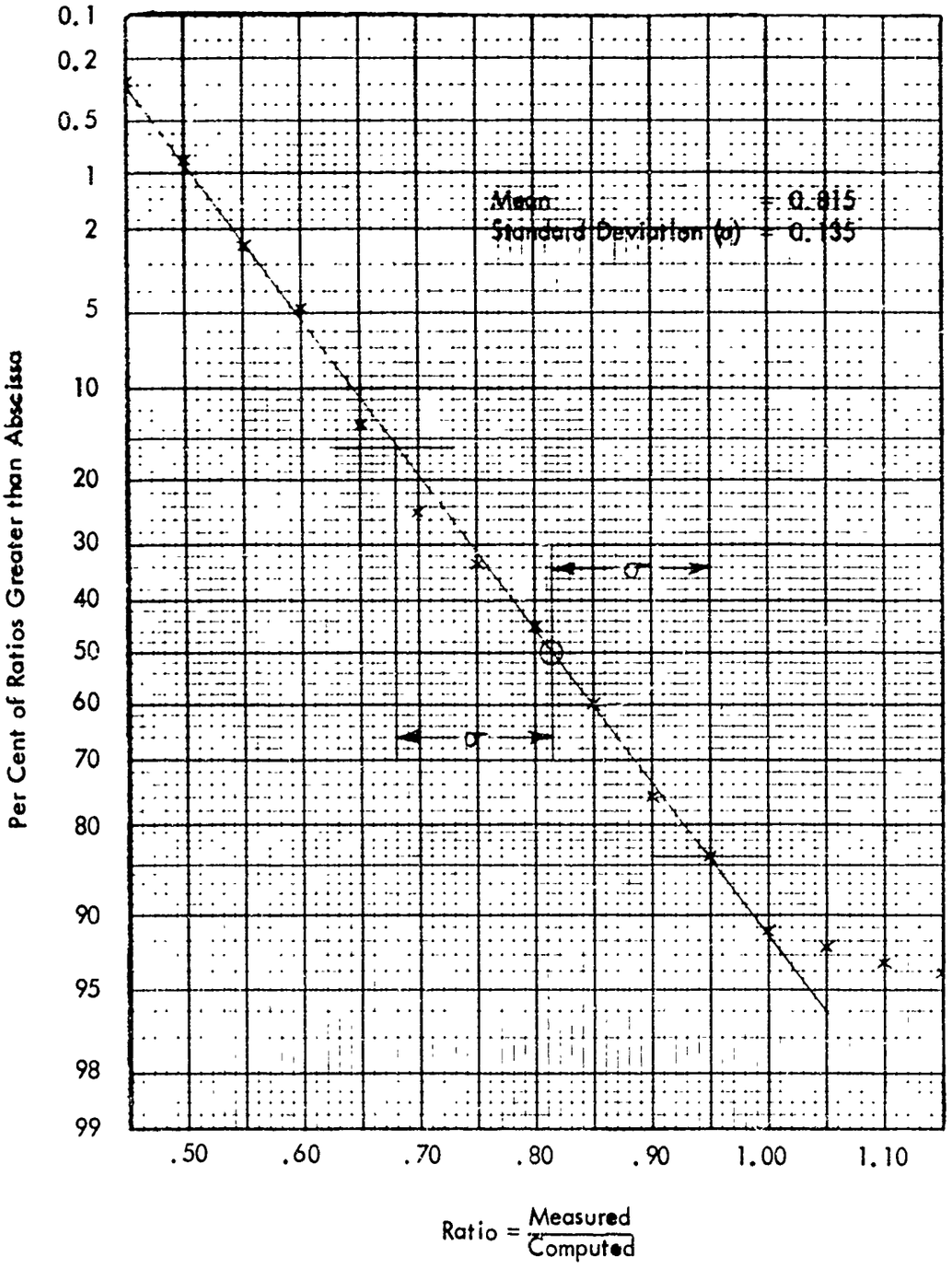

Probability Analysis

Figure 10

of parallel slant incident radiation for the values used in calculating the floor attenuation for this work at 1.25 mev is compared with that of Spencer[16] at 1.25 mev and Raso[3] at 1.00 and 2.00 mev in Figure 11 for a typical case. This figure presents the comparable attenuation curves as a function of the cosine of the slant incidence angle θ for a slab of one mean free path thickness. This latest work of Berger and Morris yields lower values of attenuation (i.e., the transmitted radiation level is lower). The Berger and Morris attenuation coefficients, in general, are lower by 10 to 20 per cent than an interpolated 1.25 mev curve for Raso's work, the greatest difference occurring in the range $0.3 < \cos\theta < 0.6$. The attenuation factor $B'_0(X_f, \bar{\omega})$ proposed in this report for use in basement calculations was based on the transmission data of Raso. It was further proposed that the $B'_0(X_f,\bar{\omega})$ results be reduced by a factor of 0.815 to bring theory and experiment into closer agreement. If Berger and Morris transmission data had been used in place of Raso's, the theoretical value of $B'_0(X_f,\bar{\omega})$ would have agreed much more closely with experiment without the 0.815 factor. This confirms the necessity of the 0.815 reduction factor to bring the analysis in line with experiment.

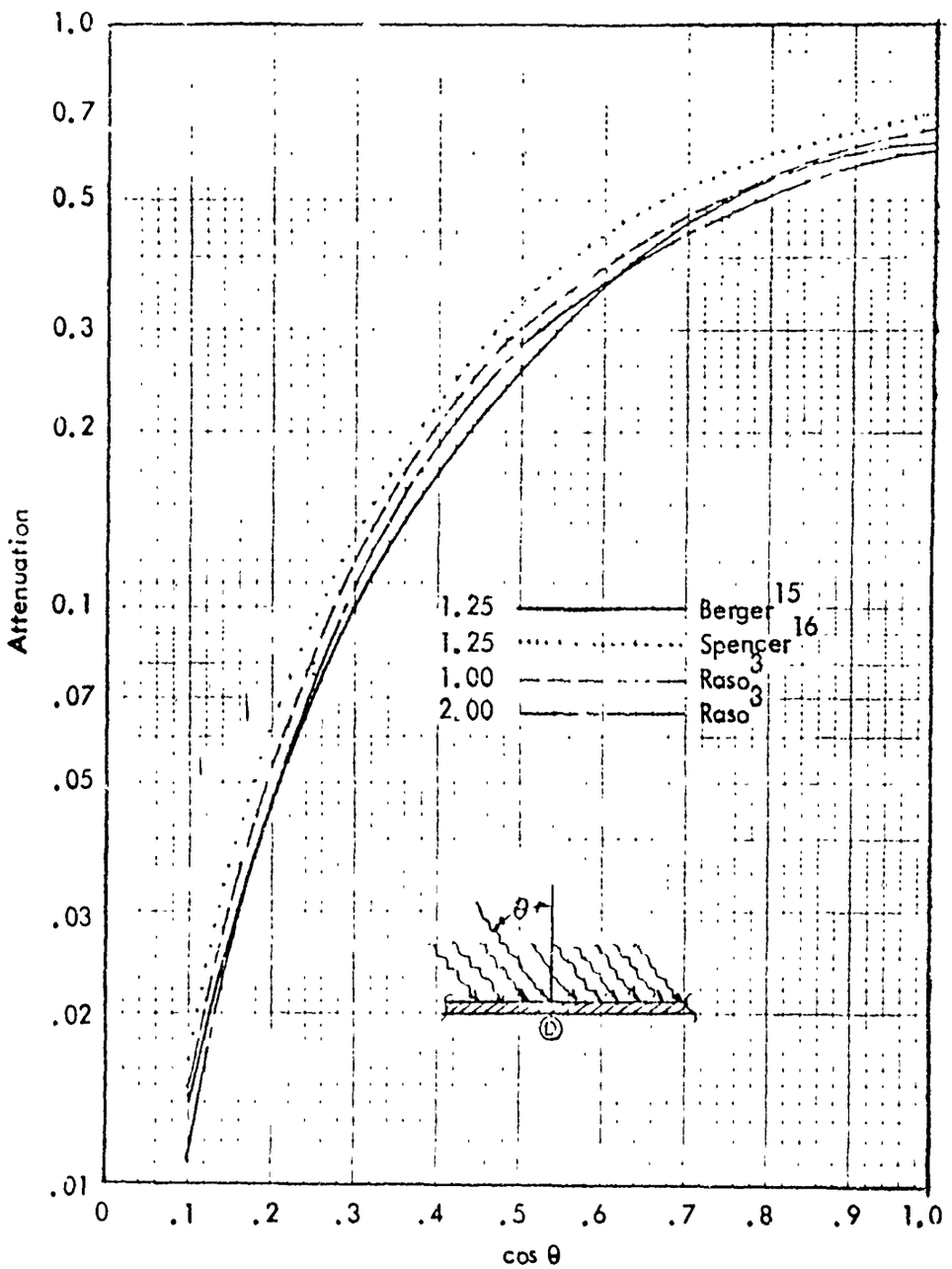

Attenuation of Parallel Slant Incident Radiation by a Slab of One Mean Free Path Thickness

Figure 1'

Supplement to TR-20-Vol. 2

CHAPTER 3

DRAFT SUPPLEMENT TO TR-20 Vol. 2 and PM100-1 FOR IN AND DOWN CORRECTION

IMPROVED BASEMENT CALCULATION

INTRODUCTION

Recent studies have indicated that more accurate protection factors may be achieved in basement areas if the attenuation of the basement ceiling is considered to be a function of both ceiling thickness and structure size. In this memorandum we shall summarize briefly the method of calculating the attenuation provided by a basement ceiling and will provide the charts and graphs necessary to make this calculation.

Floor Barrier Corrections, $\Delta X_w(X_f)$

In the current edition of the equivalent building method, the floor barrier effect is represented only as a function of the floor thickness. Recent experiments indicate that, in some cases, this interpretation may be somewhat in error. New barrier functions providing much better agreement have been computed by assuming single Compton scatter energy loss in the structure walls and attenuation similar to that experienced by parallel slant incident photons through the floor slab. Floor barrier effect thus becomes a function of both floor thickness and structure area.

Figure II-1 of TR-20 Vol. 2 indicates that the basement P_f charts are based on a floor barrier of 1.0 or, equivalently, a mass thickness of zero for the floor above the detector This was done so that any corrections would be additive. The effect of basement ceiling thickness in attenuating radiation from ground-based sources of contamination is presented in auxiliary charts, one for each basement area.

New figures replacing Charts 5 through 9 of TR-20, Vol. 2 accompany this supplement. When these charts are used to compute P_f for a bsement location, the auxilary charts on the upper portion of the figure must be used to correct for the barrier effect of the floor above the detector. The auxiliary charts were derived by converting for each building area the attenuation values computed as described above to equivalent weight of wall barrier factor B_e from Chart 2 of the Engineering Manual (TR-20, Vol. 1).

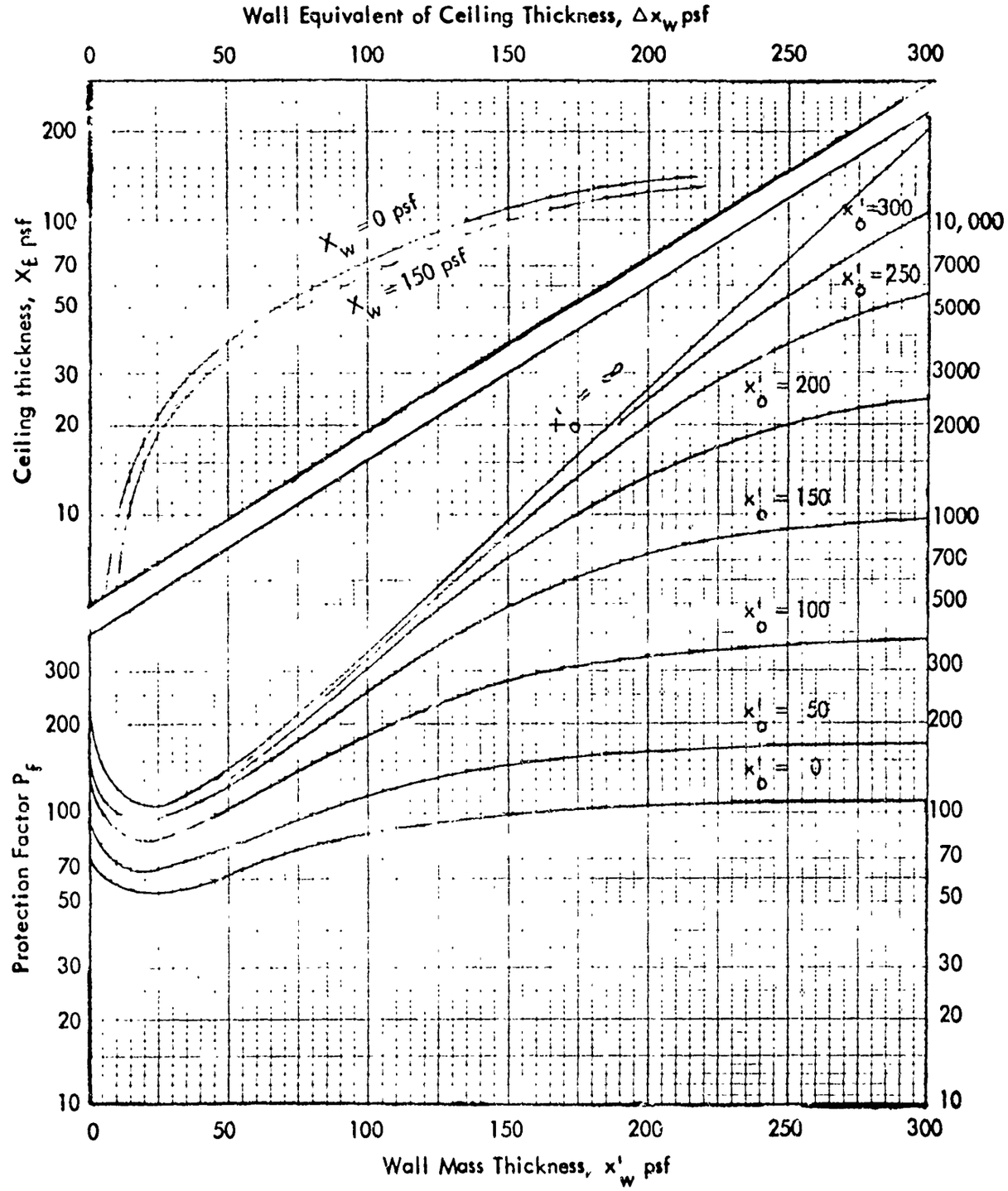

Chart 5

PROTECTION FACTOR BASEMENT: AREA = 100 sq. ft.

Figure 12

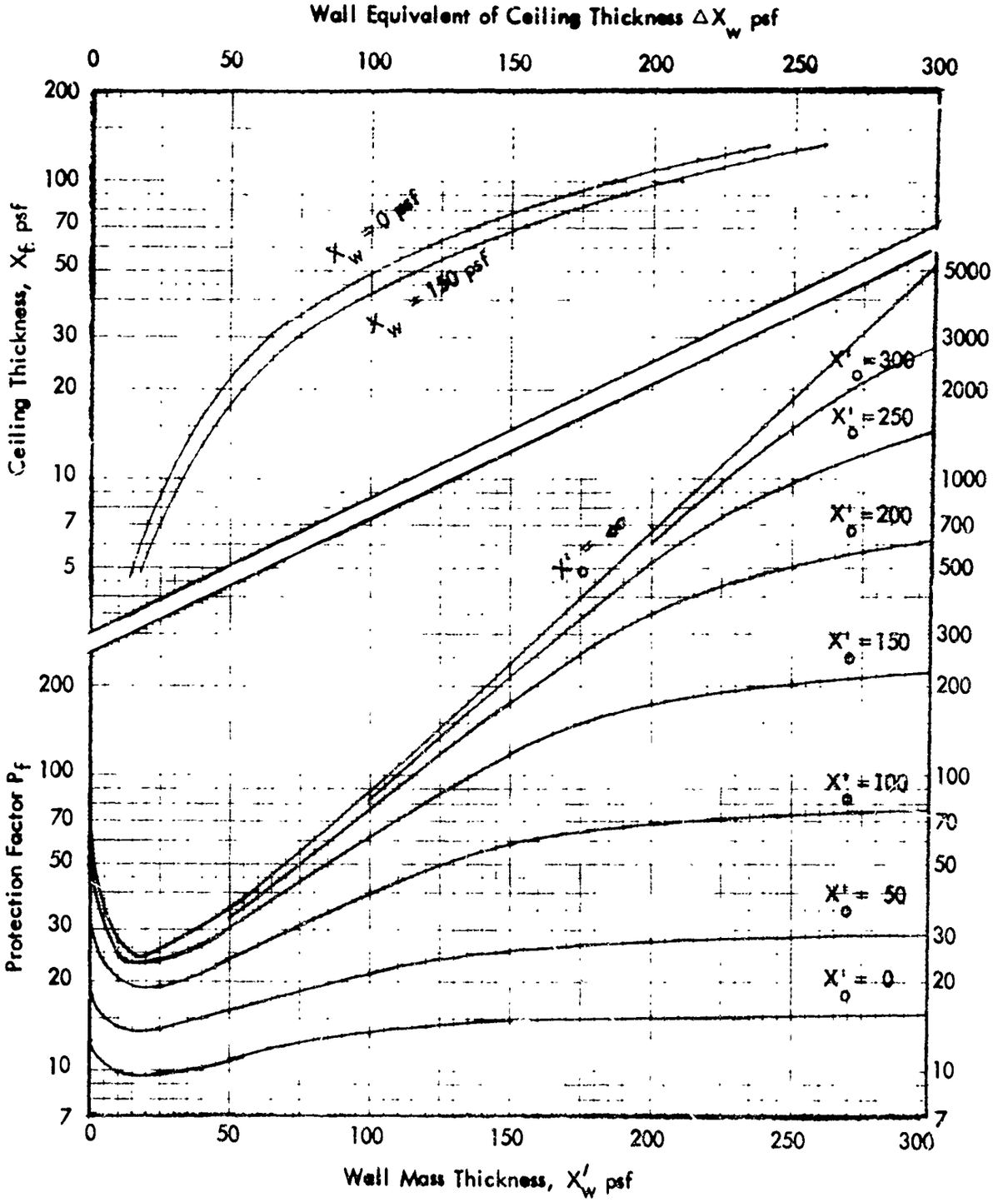

Chart 6

PROTECTION FACTOR BASEMENT: AREA = 1000 sq. ft.

Figure 13

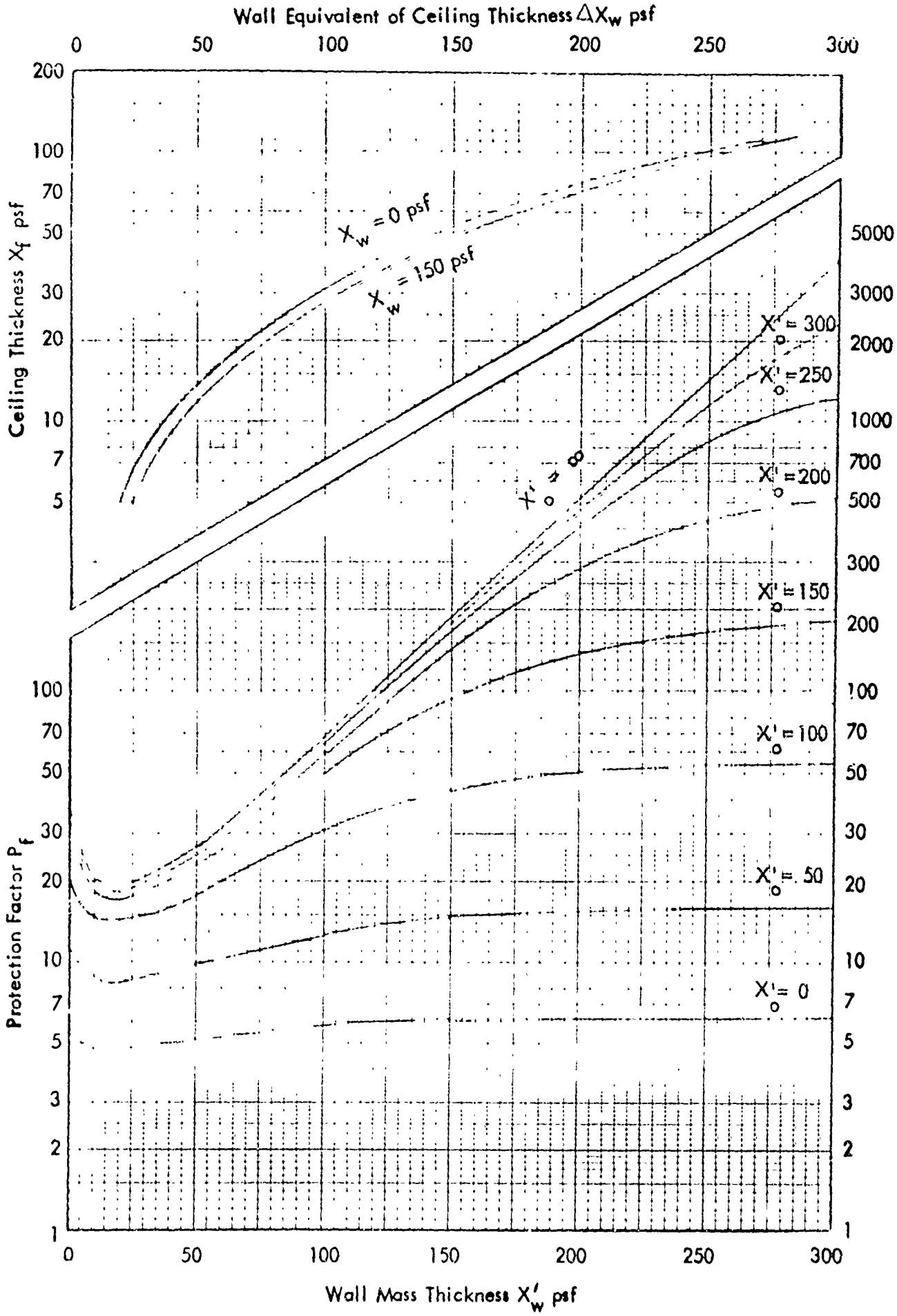

Chart 7

Figure 14 PROTECTION FACTOR BASEMENT AREA: = 4000 sq. ft.

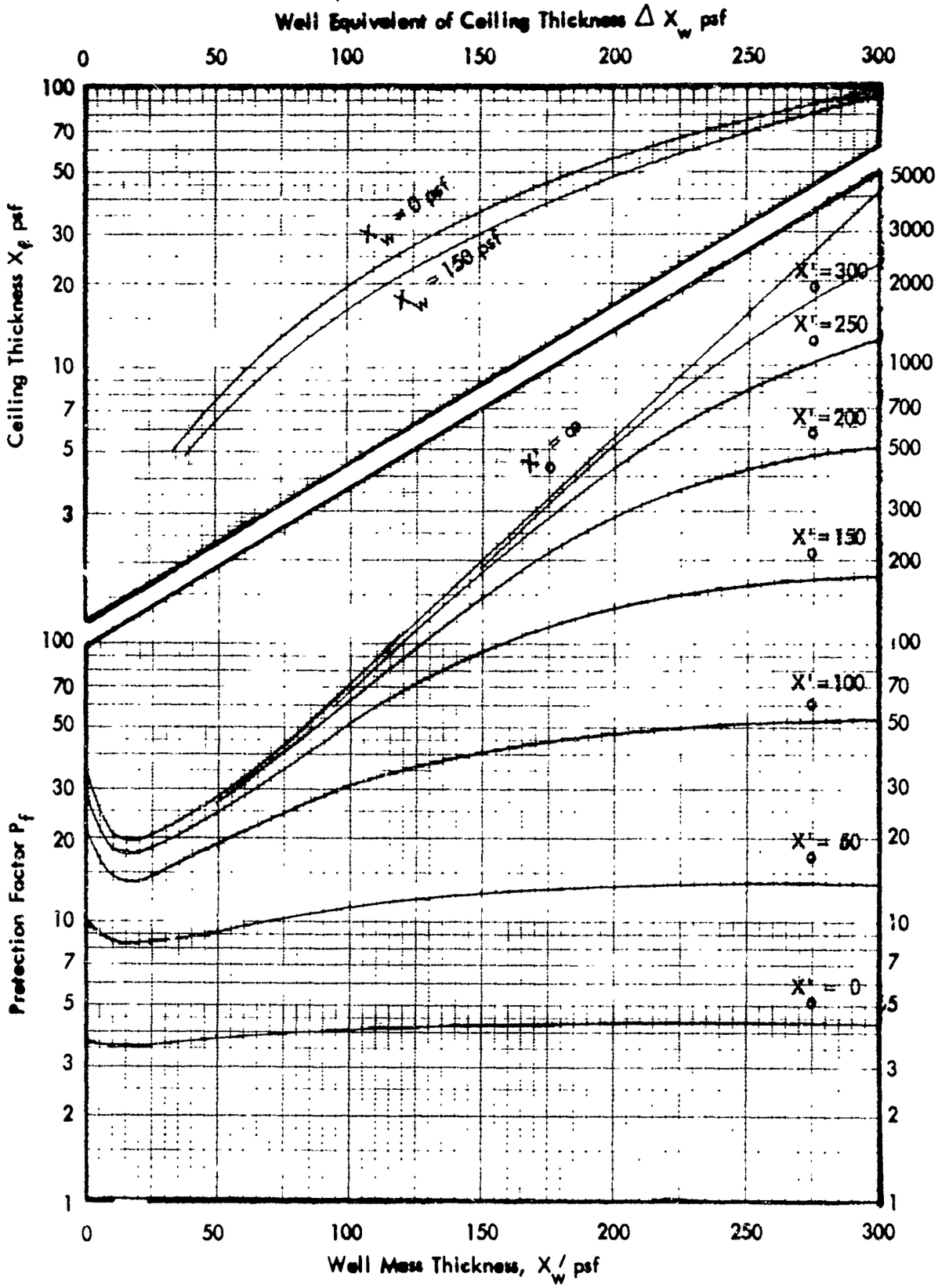

Chart 8

PROTECTION FACTOR BASEMENT: AREA = 10,000 sq. ft.

Figure 15

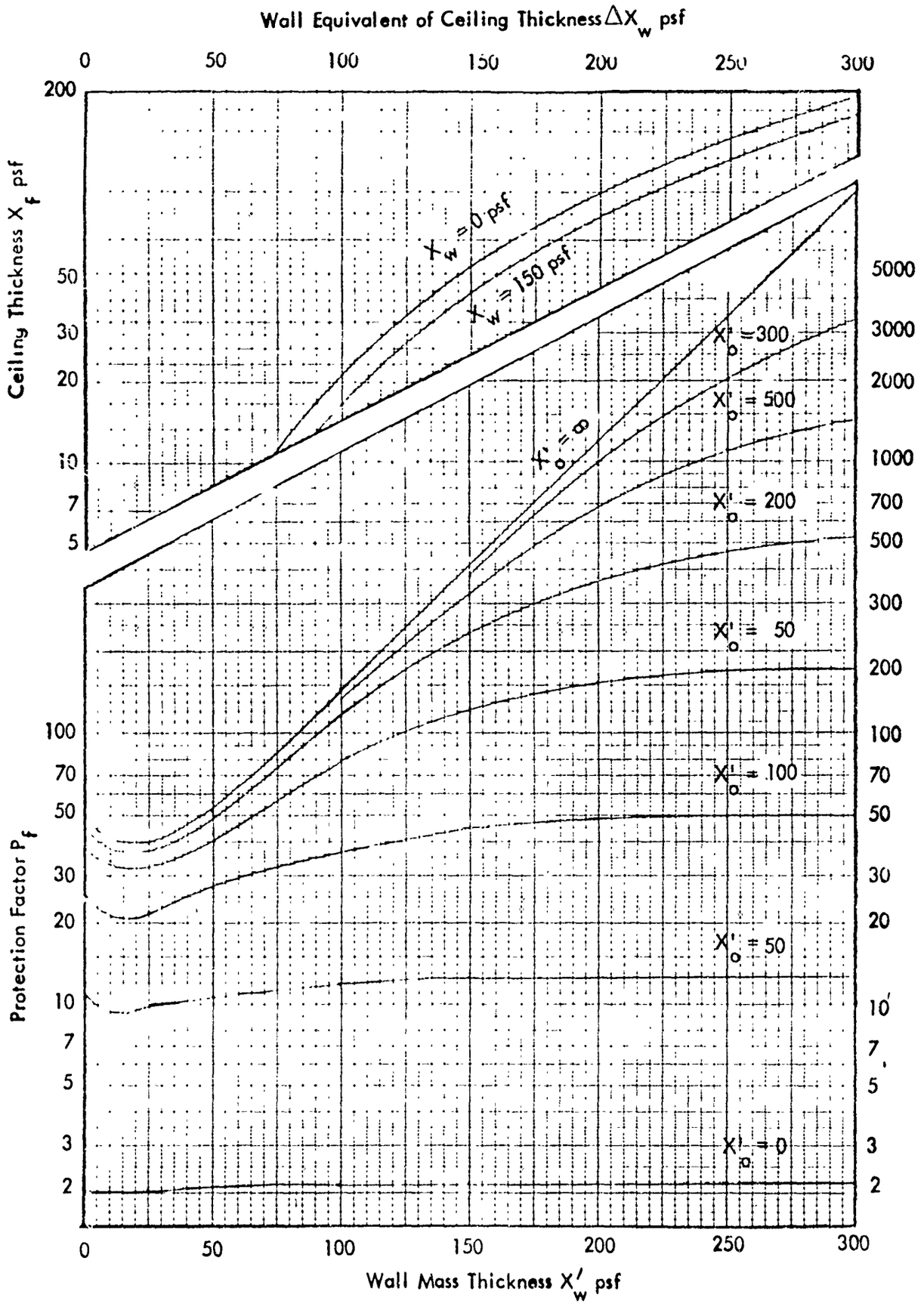

Chart 9

Figure 16 PROTECTION FACTOR BASEMENT AREA: = 100,000 sq. ft.

Illustrative Example

What is the protection factor in the basement for a rectangular building 90 ft. wide by 110 ft. length.

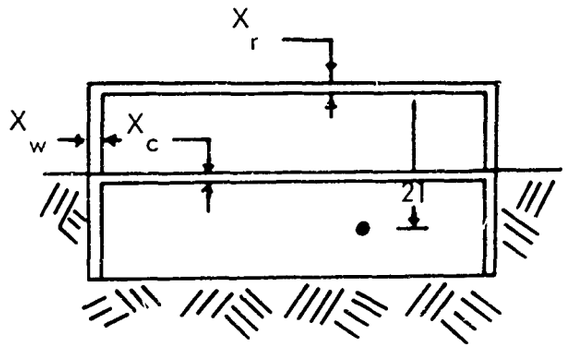

Floor thickness X_f = 50 psf
Wall thickness X_w = 70 psf
Roof thickness X_r = 100 psf

Solution:

Building area = 90 x 110' = $9900^2 \simeq$ 10,000 sq. ft.; therefore, Chart 8

Equivalent basement area $A_B = 9900\left(\frac{10^2}{17}\right)$ = 3,430 sq. ft.

Equivalent roof area $A' = 9900\left(\frac{10^2}{21}\right)$ = 2250 sq. ft.

Therefore, from Chart 16 (TR-20 - Vol. 2), equivalent roof thickness = 152 psf
Wall equivalent ceiling thickness $\Delta X_\omega\ (X_f)$ = 195; Chart 8, top
Enter Chart 8 with x_w = 70 + 195 = 265 psf and X_o = 152

Read Protection Factor, P_f = 180

Supplement to PM 100-1

TR 20 Vol. 1

DRAFT

IMPROVED "IN AND DOWN" CORRECTION

INTRODUCTION

Recent studies have indicated that protection factors of higher accuracy may be achieved in basement areas if the attenuation of the basement ceiling is considered to be a function of both ceiling thickness and structure size. In this memorandum we shall summarize briefly the method of calculating the attenuation provided by a ceiling and will provide a new chart of floor barrier factor for ground contributions through the floor above the detector to make this calculation possible.

Floor BarrierFactor, B'_o

In the current edition of the professional manual entitled "Shelter Design and Analysis, TR-20 - Volume 1, Fallout Protection and PM-100-1, Design and Review of Structures for Protection from Fallout Gamma Radiation," the attenuating effect of the floor slab is represented as a function of only the floor thickness. Recent experiments indicate that in some cases this interpretation may be somewhat in error. New barrier functions providing much better agreement have been computed by assuming single Compton scatter energy loss in the structure walls and attenuation similar to that experienced by parallel slant incidence photons through the floor slab. Floor attenuation B'_o thus becomes a function of both floor thickness and structure geometry.

This new attenuating function, $B'_o(X'_o,\omega)$, replacing $B'_o(X'_o)$, is used in the same way as that previously used. The expected dose rate in a structure from wall-scattered sources of radiation is computed for a floor slab of zero thickness and then multiplied by the attenuation introduced by the floor. Since the attenuation afforded by the floor is a function of the solid angle fraction of the scattering mass relative to the protected position of interest, as well as the floor thickness (see the figure accompanying the illustrative example), an exact calculation would require averaging over the total scattering wall from ω_u to ω'_u. An approximate method that provides excellent agreement with this more exact procedure is to determine and use a value of attenuation $B'_o(X'_o,\omega)$ for the arithmetic average of the solid angle fraction describing the scattering surface.

As in the illustrative example, the attenuation introduced by the floor would be equivalent to $B'_o(X'_o, \bar{\omega})$, where:

$$\bar{\omega} = \frac{\omega_u + \omega'_u}{2}$$

Illustrative Example (Reference Example 4-5, PM100-1) and Example 5.2 TR-20 (Vol. 1)

Simple basement of multistory structure. Negligible roof contribution

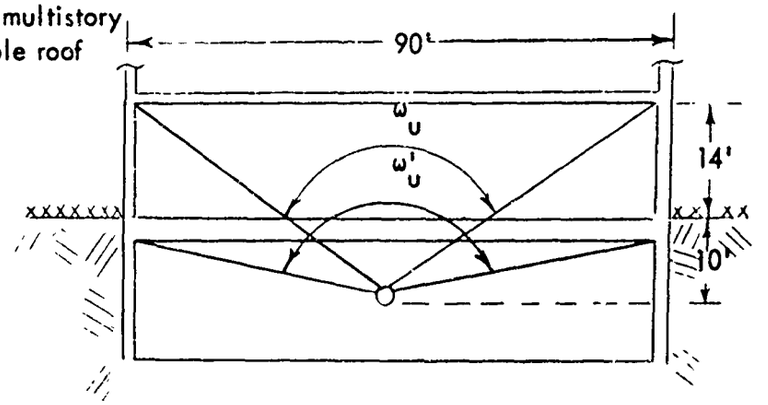

W = 90 ft
L = 110 ft
X_e = 70 psf
X_c = 50 psf
X'_o = 450 psf

The required protection factor for this building

1. Functional equations

C_o = negligible because X_o is greater than 350 psf

$$C_g = \left[B(X_e,h)\, B'_o(X_c,\bar{\omega}) \left\{\left[G_a(\omega_u) - G_a(\omega'_u)\right]\left[1-S_w(X_e)\right] + \right.\right.$$

$$\left.\left. + \left[G_s(\omega_u) - G_s(\omega'_u)\right]\, S_w(X_e)\, E\,(e)\right]\right\}$$

2. Determining solid angle fractions and parameters

						Chart 3*	Chart 5*	Chart 5*
ω	W	L	Z	e	n	ω	$G_a(\omega)$	$G_s(\omega)$
ω_u	90	110	24	.82	.44	.60	.079	.33
ω'_u	90	110	10	.82	.18	.82	.051	.19

$$\bar{\omega} = \frac{\omega_u + \omega'_u}{2} = \frac{.60 + .82}{2} = 0.71$$

$B'_o(X_c, \bar{\omega}$ = B'_o (50, 0.71) = 0.029 Accompanying chart (Fig. 17)

$B_e(X_e, h)$ = B_e(70,3) = 0.18 Chart No. 2*

$S_w(X_e)$ = S_w(70) = 0.66 Chart No. 7*

E(e) = E(.82) = 1.41 Chart No. 8*

*Chart of PM100-1

3. Solution:

$$C_g = (0.18)(0.029)\left\{\left[(.079 - .051)(1-.66) + \left[.33 - .19\right]\left[.66\right]\left[1.41\right]\right\}\right.$$

$C_g = .00073$

$R_F = C_g + C_o = .00073 + .00000 = .00073$

$P_F = 1/R_F = 1/.00073 = 1370$ say 1300 answer

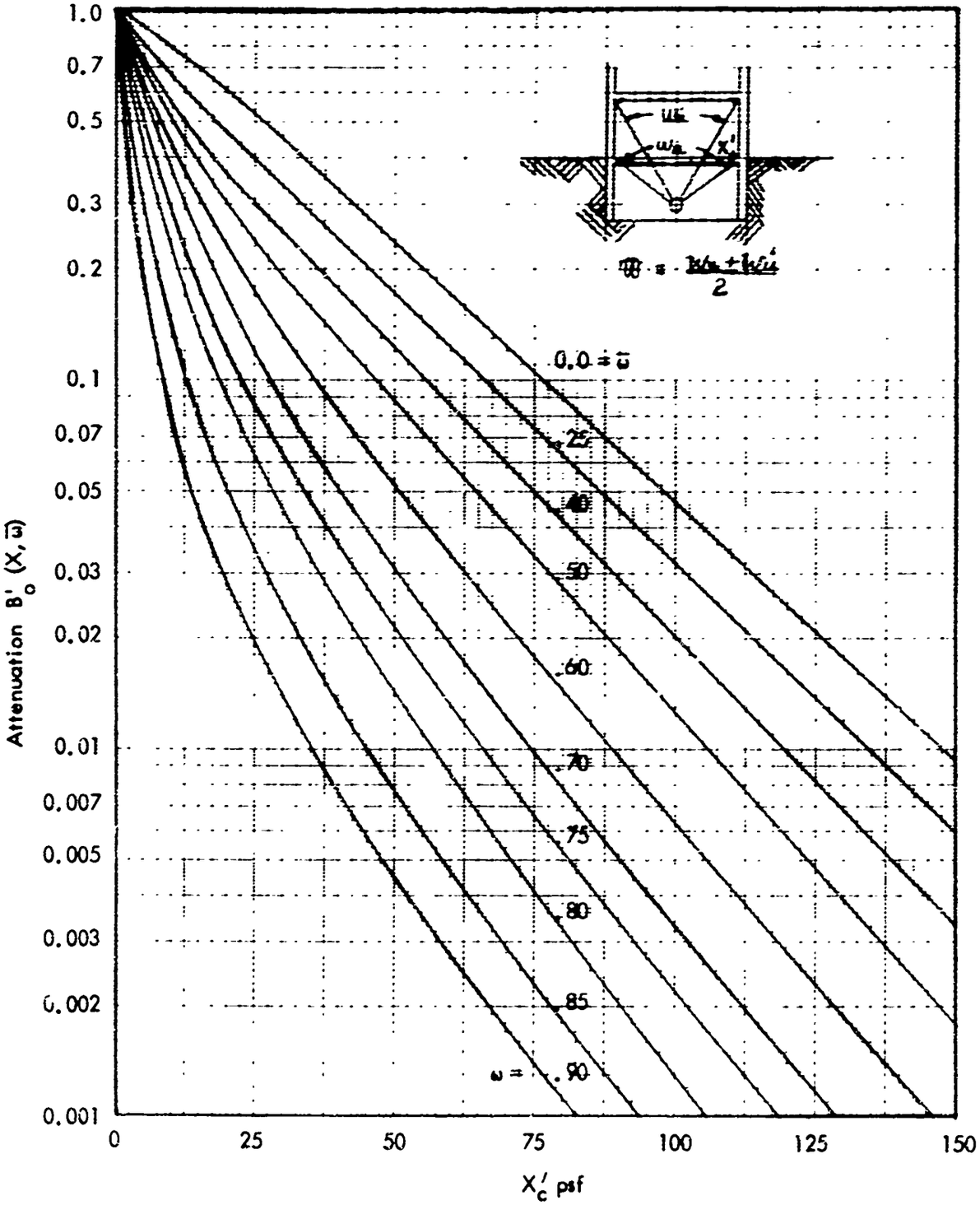

Recommended Floor Attenuation Values
1.12 Hour Fallout Spectrum

Figure 17

Illustrative Example 2 - Ref. Example 5.3,
TR-20 (Vol. 1)

Exposed Basement Walls

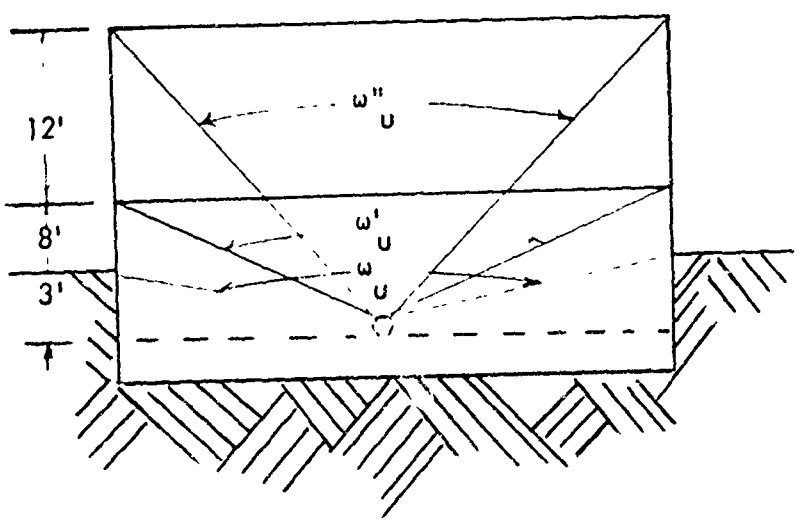

L	=	100 ft.	W = 50 ft.
X_e	=	50 psf	(first story)
X_e	=	100 psf	(basement)
X'_o	=	60 psf	
X_r	=	100 psf	

						Chart 3	Chart 5	Chart 5
ω	W	L	Z	e	η	ω	G_s	G_a
ω''_u	50	100	23	.50	.46	.47	.39	.086
ω'_u	50	100	11	.50	.22	.70	.28	.069
ω_u	50	100	3	.50	.06	.91	.11	.029

Solution:

$$\bar{\omega} = \frac{\omega'_u + \omega''_u}{2} = \frac{.70 + .47}{2} = .59$$

a.

$B_e\ (X_e, H) = .095$

$S_w\ (X_e) = .73$

$E(e) = 1.34$

$$C_g = \left\{ \left[G_a(\omega'_u) - G_a(\omega_u) \right] \left[1 - S_w(X_e) \right] + \left[G_s(\omega'_u) - G_s(\omega_u) \right] S_w(X_e)\, E(e) \right\} B_e(X_e, H)$$

$$C_g = \left[(.069 - .029)\,(1 - .73) + (.28 - .11)\,(.73)(1.34) \right] .095$$

$$C_g = .0168$$

b. First-Story Walls

$$C_g = \left\{\left[G_a(\omega''_u) - G_a(\omega'_u)\right]\left[1 - S_w(X_e)\right] + G_s(\omega''_u) - G_s(\omega'_u)\, S_w(X_e)\, E(e)\right\} B_e(X_e, H)\, B'_o(X'_o, \bar{\omega})$$

$$S_w(X_e) = .69 \quad B'_o(X'_o, \bar{\omega}) = .037$$

$$B_e(X_e, H) = .15 \quad E(e) = 1.34$$

$$C_g = \left[(.086 - .069)(1 - .69) + (.39 - .28)(.69)(1.34)\right](.15)(.037)$$

$$C_g = .000595$$

total: $C_g = .0168 + .000595 = .0174$

c. Roof Contribution

$$X_o = X_r + X'_o = 160 \text{ psf}$$

$$C_o(\omega''_u, X_o) = .0039$$

$$P_f = 47$$

Detector heights above ground are treated in a similar manner.

CHAPTER 4

FINITE FIELDS OF CONTAMINATION

INTRODUCTION

Many shelter areas in this country depend in part for their worth on the fact that they are subjected to limited rather than infinite fields of contamination. A common situation, that of row housing in urban areas, for example, would subject the sheltering structures to radiation originating from a finite field of contamination perhaps 50 ft. wide on both sides of the structure. These structures would then be as much as three times more effective than an identical structure surrounded by a full field of contamination. Parker[17] estimates that fully half of the basement shelter areas surveyed at the time his report was published were subjected to field widths of less than 60 ft.

Two areas of inquiry arise when we evaluate the methods currently used in predicting the effects of finite fields of contamination. We must first determine if the more detailed method of calculation as represented by the "engineering method" adequately portrays the physical situation. Second, we must ask whether or not the simplified "equivalent building method" agrees with results obtained by means of the more complex method. The agreement between the two methods in their present form has been examined[1] previously and recommendations for improving upon this agreement have been made. The required changes have been held in abeyance until an adequate answer to the first area of inquiry (the accuracy of the more complex method of calculation) has been determined. Our purpose in this chapter is to examine this accuracy by comparing it with the best information available.

There are few experimental data with which to evaluate the methods proposed for computing the shelter afforded against finite fields. Several years ago, an experiment was conducted to determine the effect of finite fields of contamination on above-ground locations. This experiment used the modeling technique, with iron as the attenuating medium, and simulated contamination in the form of rectangular areas. Eisenhauer[4] analyzed these data in detail, concluding that "comparison of experimental and calculated results shows good agreement for both structures except for the first story." A second, brief experimental series, conducted on full-scale concrete structures by McDonnell, using circular annuli, again indicated fair agreement between experiment and theory. Both experiments were exclusively for upper-story locations, where both direct and scattered radiation affected the dose measured in approximately equal amounts. Since neither of these experimental series was rigorous in the examination of finite fields of contamination and because so many shelter areas seem to be affected only by finite fields of

contamination, a further evaluation was undertaken. Eisenhauer[20] recently completed a computer compilation program, using Berger and Morris' Monte Carlo transmission coefficients[15] for 1.25 mev prediction. This program is capable of computing the radiation originating from any arbitrarily located square patch of contamination through any rectangular wall area to an arbitrarily located detector. The program, therefore may be used to generate numerical "experiments" with which to compare the existing calculational method.

The Engineering Method of Shelter Computations from Finite Contamination Fields

The engineering method of shelter computation described in the manual "Design and Review of Structures for Protection from Fallout Gamma Radiation"[9] presents rules for computing the ground-based dose contributions for structures subjected to radiation from both infinite and limited fields of contamination. In this method the radiation arriving at a point within a structure is subdivided into three components: radiation that (1) has passed directly through the building walls without scattering, (2) has been scattered by the walls, and (3) has been scattered by the atmosphere. Non-wall scattered or direct radiation from an infinite field of contamination is determined by multiplying the cumulative angular distribution of non-wall scattered radiation, $G_d(\omega,h)'$ as viewed from the point of interest in the structure by the height-dependent wall barrier factor $B(X_e,h)$, and by the fraction of radiation not scattered by the structure walls, $(1-S_w)$. Calculations for the finite field case are similar except that the cumulative angular distribution of non-wall scattered radiation must be differenced to account for the finite field.

The wall-scattered component for an infinite field case is determined by multiplying the cumulative angular distribution of radiation scattered from the structure walls, $G_s(\omega)$, by the height-dependent wall barrier factors $B(X_e,h)$ the shape correction factor, (E), the fraction of emergent radiation scattered, (S_w), and a floor barrier factor, $B_o(X_f)$ or ceiling factor, $B'_o(X_c)$, where applicable. The floor barrier factor is used for attenuating wall-scattered radiation reaching the detector from the floor below in a multistory structure whereas similarly, the ceiling barrier factor is used for wall-scattered radiation reaching the detector from the story above For a finite field case this procedure is modified by applying a different wall barrier factor, $B_{\omega s}(\omega_s, X_e)$, which is expressed as a function of the solid angle of the field of contamiation as viewed from the structure's wall at midstory height in place of the infinite-field wall-barrier factor, $B(X_e,h)$.

The atmospheric scattered component for both the finite and the infinite field of contamination cases are determined by multiplying the cumulative angular distribution of skyshine radiation, $G_a(\omega)$, , by the wall barrier, $B(X_e,h)$, the fraction of radiation not scattered in passing through the structure walls, $(1-S_w)$, and the ceiling barrier, $B'_o(X_e)$, when appropriate. The assumption that the

atmospheric scattered component for a finite field is nearly identical to that of the infinite field case should, in practice, be fairly accurate. Though adjacent buildings may block the direct view of part of the field of contamination, however, the air-scattered radiation physically blocked by the adjacent buildings will be approximately balanced by radiation scattering from the walls of these buildings. Also, it is expected that in most realistic cases there will be fallout on the tops of the adjacent buildings as well as in the region behind them; hence the angular distribution of the radiation that is not blocked by adjacent walls will remain the same.

The three radiation components: direct, wall-scattered, and air-scattered, are then summed to give the total dose contribution. The general equation for the total ground contamination within a multistory structure in a limited field of contamination is presented, together with a sketch of the idealized building arrangement, in Figure 18.

Charts in the Engineering Manual[9] for determining the geometric and barrier reduction factors used in structure shielding calculations were derived from the basic data on radiation penetration developed by Spencer[16] for 1.12 hr. fallout. Chart 7 in the manual, for the fraction of emergent radiation from a wall barrier that is scattered, (S_w), is, however, for Cobalt-60 radiation. Since most experimental verifications of the Engineering Manual calculation procedures have been and are being performed using Cobalt-60 radiation, and since the NBS computer compilation program[20] against which we wish to compare the engineering method uses the 1.25 mev (Cobalt-60) Monte Carlo transmission coefficients of Berger and Morris, the Engineering Manual method has had to be extended to 1.25 mev radiation in order to permit accurate comparisons. Cobalt-60 curves for the barrier shielding reduction factors, $B_o(X_f)$ $B_o(X_e,3')$, and $B'_o(X_c)$ are presented in Figure 19a. The data in this figure has been calculated in the same way and are equivalent to Chart 1 of the Engineering Manual, in which Case 1 applies to a horizontal floor barrier, $B_o(X_f)$, Case 2, the exterior vertical wall barrier, $B(X_e,3')$, and Case 3, an overhead or ceiling horizontal barrier, $B'_o(X_c)$. Figure 19b presents the Cobalt-60 overhead or ceiling horizontal barrier $B'_o(X_c)$. Figure 19b presents the Cobalt-60 exterior wall attenuation effects for detector heights to 300 ft., and is equivalent to the Chart 2 fallout curves of the Engineering Manual. Cobalt-60 directional responses from ground sources of contamination G_d, G_s, and G_a are given in Figure 20a, which has been calculated in the same way and therefore is equivalent to Chart 5 of the Manual for 1.25 mev radiation. Figure 20b similarly extends the directional response for direct radiation G_d to detector heights of up to 100 ft., and is equivalent to Chart 6 of the Manual.

Barrier shielding effects $B'_o(X_f)$, $B_e(X_e$, and $B'_o(X_c)$ for Cobalt-60, as given in Figures 19a and 19b, were developed directly from Spencer's[16] L(X), 2W(X,d), and S'(X) curves respectively, and agree closely with those developed by LeDoux.[21]

Ground dose = (non-wall scatter, detector story) + (skyshine, detector story) + (wall scatter, detector story)
+ (non-wall scatter, through story below detector) + (wall scatter, through story below detector story)
+ (wall scatter, through story above detector) + (skyshine, through story above detector)

$$D_o = B(x_e,h)\left[G_d(\omega_\ell,h) - G_d(\omega_\ell^*,h)\right](1-Sw) + B(x_e,h)\,G_a(\omega_u)(1-S_w) + B_{\omega s}(\omega_s, x_e)\left[G_s(\omega_\ell) + G_s(\omega_u)\right] S_w E$$

$$+ B_o(x_f)\,B(x_e,h)\left[G_d(\omega'_\ell,h) - G_d(\omega_\ell,h)\right](1-S_w) + B_o(x_f)\,B_{\omega s}(\omega_s, x_e)\left[G_s(\omega'_\ell) - G_s(\omega_\ell)\right] S_w E +$$

$$+ B'_o(x_c)\,B_{\omega s}(\omega, x_e)\left[G_s(\omega'_u) - G_s(\omega_u)\right] S_w E + B'_o(x_c)\,B(x_e,h)\left[G_a(\omega'_u) - G_a(\omega_u)\right](1-S_w)$$

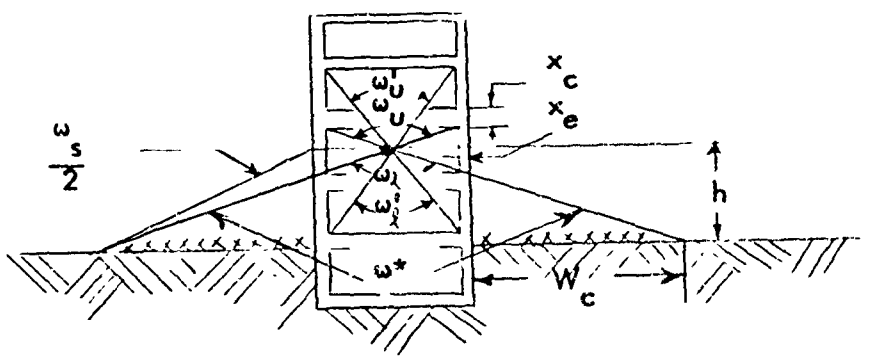

LIMITED FIELD EQUATION FOR ENGINEERING TECHNIQUE

Figure 18

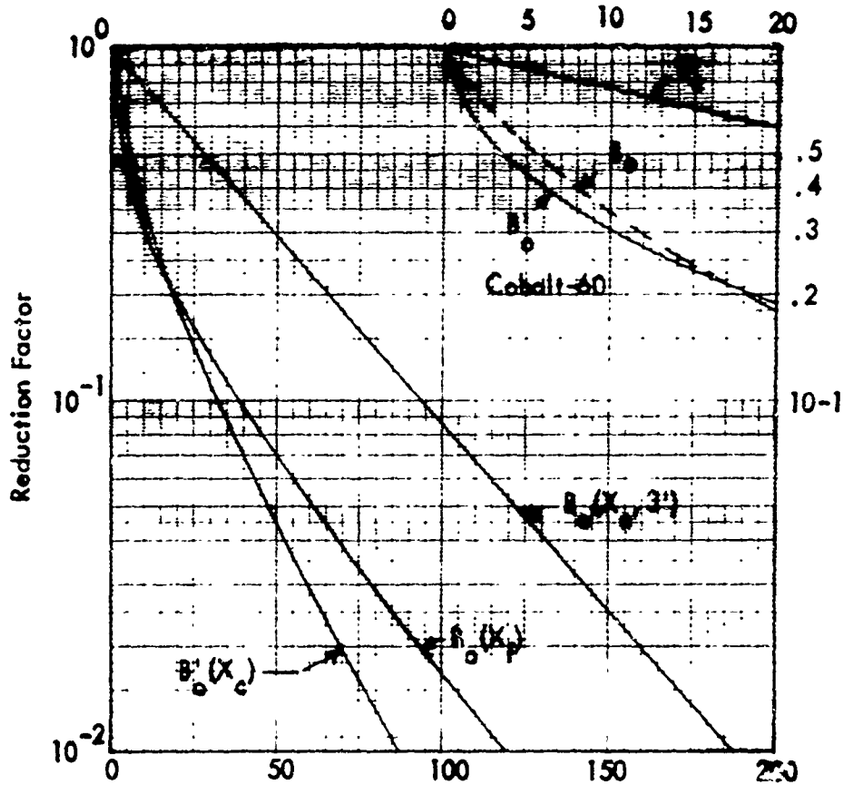

Barrier Shielding Effects B_o, B_e, and B'_e

Figure 19a

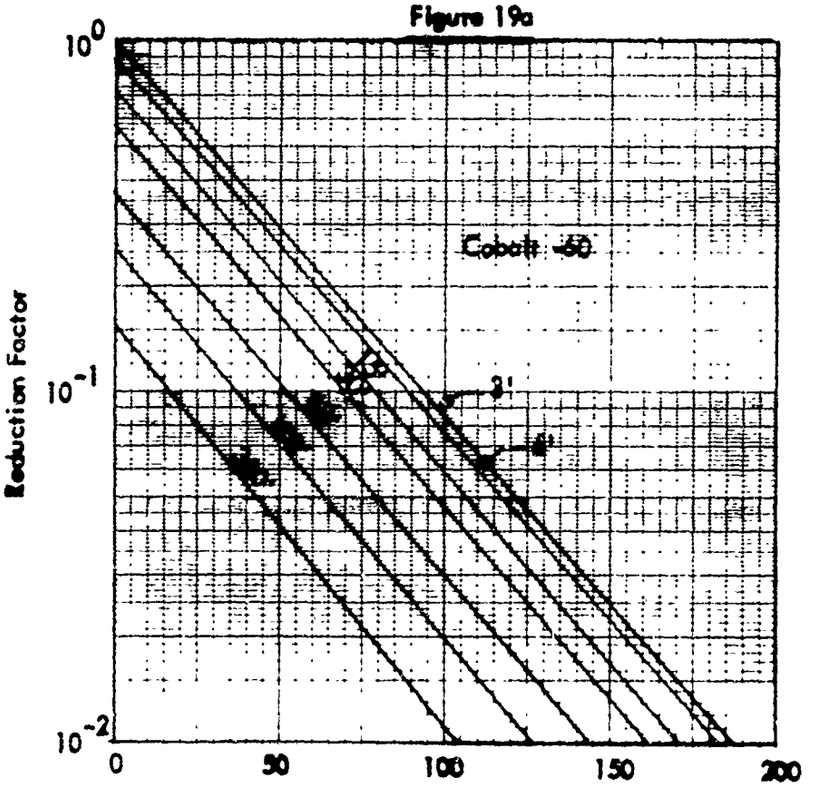

Wall Barrier Shielding Effects, $B(X_e)$ for Various Heights

Figure 19b

Figures 20a and 20b for directional response $G_d(\omega,h)$, $G_s(\omega)$ and $G_a(X)$ were developed from the basic work of Spencer.[16] LeDoux[21] also has developed Cobalt-60 curves for the directional responses, which in general agree well with the curves of Figure 20 except for values of G_d at detector heights above 3 ft.

Values for the direct angular distribution $G_d(\omega,h)$ in Figures 20a and 20b were developed from the equation:

$$G_d(\omega,h) = \frac{\int_{-1}^{\cos\theta_\lambda} \lambda(d,\cos\theta)d(\cos\theta)}{\int_{-1}^{1} \lambda(d,\cos\theta)d(\cos\theta)} = \frac{\int_{-1}^{1} \lambda(d,\cos\theta)d(\cos\theta) - \int_{-1}^{0} \lambda(d,\cos\theta)d(\cos\theta) - \int_{\cos\theta\lambda}^{1} \lambda(d,\cos\theta)d(\cos\theta)}{\int_{-1}^{1} \lambda(d,\cos\theta)d(\cos\theta)}$$

which in Spencer's[16] notation is identically equal to

$$G_d(\omega,h) = 1 - \frac{S(d)}{L(d)} - L_a(d,\omega)$$

where $\lambda(d, \cos\theta)$ is the angular distribution and S(d), L(d), and $L_a(d,\omega)$ for Cobalt-60 are taken from Spencer's[16] work. S(d) divided by L(d) is the ratio of skyshine to total radiation at a distance d above a uniform infinite source field. G_s(cobalt) was calculated from the equation used for G_s(fallout), using $S_a(d,\omega)$ curve for Cobalt-60 at d = 3 ft. Thus:

$$G_s = 0.5\,(1-S_a(d,\omega)$$

Similarly, the cumulative skyshine contribution

$$G_a = 0.168\,G_s(\omega)\quad 1 + (1/2 - G_s(\omega)\ \}$$

where 0.168 is twice the skyshine fraction of the total radiation at 3 ft. altitude.

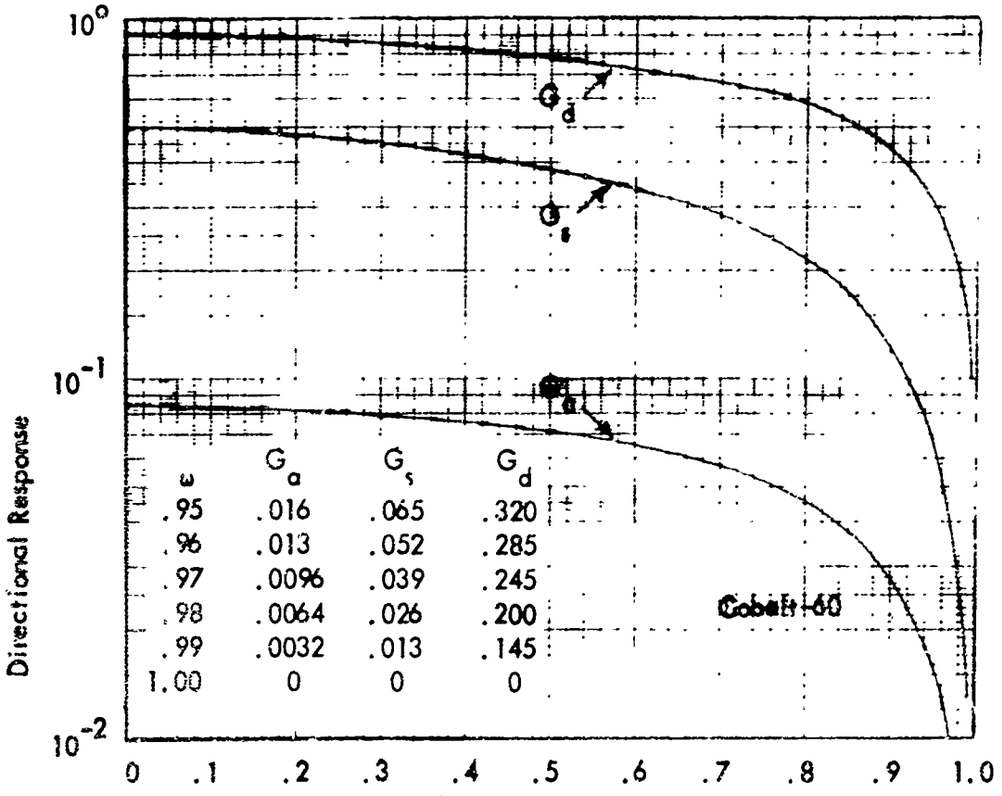

ω	G_a	G_s	G_d
.95	.016	.065	.320
.96	.013	.052	.285
.97	.0096	.039	.245
.98	.0064	.026	.200
.99	.0032	.013	.145
1.00	0	0	0

Directional Response, Ground Contribution, G_d, G_s, G_a

Figure 20a

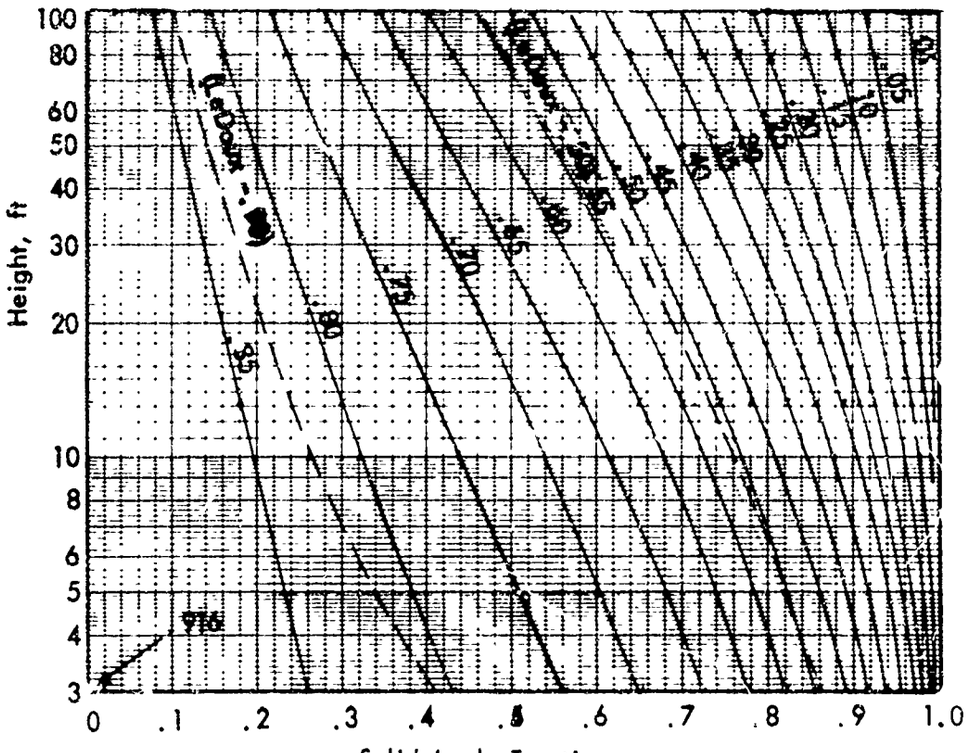

Directional Response, G_d for Various Heights

Figure 20b

Agreement for $G_d(\omega,3')$ between values calculated in this manner and curves developed by LeDoux are excellent up to $\omega = .90$. For values of $\omega > .90$, the values of Figure 20 are somewhat higher than those of LeDoux (for example, at $\omega = .99$, G_d (Figure 20) = .14, G_d(LeDoux) = .105). Similarly, agreement for the cumulative angular distribution of wall-scattered radiation G_s between Figure 20 and values previously derived by LeDoux is excellent, Conesco values being slightly higher at ω .75 (for example, at $\omega = .99$, G_s(Figure 20) = .013, G_s (LeDoux) = .011). The skyshine cumulative angular distribution G_a also shows good agreement between the values shown in Figure 20 and those previously derived by LeDoux, with values of Figure 20 slightly less for ω .75 and slightly higher for ω .75. Figure 20b presents the direct response G_d for heights to 100 ft. and agrees fairly well with values developed by LeDoux. Agreement at $G_d(\omega, 3')$ as discussed above, was good. Agreement at heights greater than 3 ft, however, is not as good, particularly at small values of ω. This is illustrated in Figure 20 by including both curves at $G_d(\omega,h)$ equal to 0.50 and 0.75.

Engineering Manual Chart 9, used for obtaining the finite field wall barrier factor $B_{\omega_s}(\omega_s, X_e)$ is for 1.12 hr. fallout. Fallout values for $B_{\omega_s}(\omega_s, X_e)$ were used in this study for calculating 1.25 mev structure reduction factors for comparison with the computer Monte Carlo results. This was done for two reasons: (1) a Cobalt-60 barrier chart for limited strips of contamination had not been developed at the time this study was conducted; (2) the error introduced by using the fallout chart values in place of Cobalt-60 should be small at the mass thickness (9, 36, and 144 psf) used in this study. The error in the finite wall-barrier factor in using fallout values instead of Cobalt-60 can be approximated by considering the differences between fallout and Cobalt-60 infinite field wall barrier factors. For the infinite field case the Cobalt-60 barrier factor is about 5 per cent less than the fallout value at 100 psf, and 25 per cent at 200 psf. Since the wall thickness values used in this study are 36 psf or less, except for one point at 144 psf, errors introduced are expected to be small.

Computations of the Engineering Manual type were performed using data for 1.25 mev on a series of simple structures for comparison with corresponding values determined by the NBS compilation program for finite fields. The series was based on a single-story structure of the blockhouse type. Building floor area, width-to-length ratios (eccentricity), and wall thickness were varied to provide data for a comparison with the compilation program over a wide range of structure parameters. The width of the rectangular field of contamination surrounding the structure was varied from a narrow strip only 10 ft. wide to a maximum width of 90 ft. One group of structures provided building length-to-width ratios from 1 to ∞. The bases of these buildings were 20 by 20 ft., 20 by 40 ft., and 20 ft. by ∞, calculations being made for each for three wall mass thicknesses (9, 36, and 144 psf). A second group consisted of two square buildings 20 by 20 ft., and 40 by 40 ft., again computed for wall thickness values of 9, 36, and 144 psf. The building height was

10 ft. and the detector was centrally located at 5 ft. height for all cases. Computed values of the direct and scattered radiation for the two groups of structures are summcrized in Tables 5 and 6.

In certain cases the values of direct radiation presented in Tables 5 and 6 are slightly different from those which would be computed using the data of Figures 19 and 20 because the values of G_d used in computing these results varied slightly from the refined values presented in Figure 20. The differences in direct radiation caused were generally less than 10 per cent and do not affect the conclusions presented in this chapter.

Shielding calculation of the Engineering Manual type as illustrated in Figure 18, for this series of single-story structures subjected to finite rectangular fields of contamination may be simplified to the following equation:

Dose = direct radiation component + scattered radiation component

$$D_o = B(X_e,h)\left[G_d(\omega_f,h) - G_d(\omega^*,h)\right](1-S_w) + B_{\omega s}(\omega_s,X_e)\left[G_s(\omega_f) + G_s(\omega_u)\right]S_w E$$

The skyshine component is omitted from this equation so as to permit direct comparison with the NBS Monte Carlo compilation method. The NBS method neglects the effect of the atmosphere and assumes that all radiation enters through the detector story walls of the structure (i.e., there are no radiation components from the story below or above). The direct radiation attenuation factor, $B(X_e,5')$, was taken from Figure 19b, and the angular distribution, $G_d(\omega_f,5')$ and $G_d(\omega^*,5')$, generally from Figure 20b. Two complications, however, enter into the calculation of the direct radiation components as the building width/length ratio approaches zero. The first arises in calculating solid angle fractions for an infinitely long building and the second is introduced by the tacitly assumed equivalence of circular and rectangular solid angles when computing angular distributions. For an infinitely long structure, the solid angle fraction ω equals $\frac{2}{\pi}\tan^{-1}\left(\frac{W}{2Z}\right)$, where W is the structure width and Z is the detector height. As for the second complication, one finds that in differencing $G_d(\omega,h)$ for a series of buildings with fixed width and varying length and a fixed finite field width, the value of ΔG_d first decreases with increasing building length as one would expect, then as the building increases further in length, ΔG_d increases. As building length increases toward infinity the direct contribution and hence ΔG_d should asymptotically approach a minimum at a length-to-width ratio of infinity and should not increase. In the actual calculations for direct radiation for a given source field and building width, ΔG_d was plotted versus building eccentricity until the minimum was reached. Values

TABLE 5

Engineering Manual Direct and Scattered Ground Contributions (One Story Structure, 5 Ft. Detector Height, 1.25 mev Radiation)

Building (ft.)	Wall thickness (psf)	Radiation component	Field width (ft.) 10	20	30	40	50	70	90
20 x 20	9	Direct	.0739	.112	.167	.192	.212	.243	.270
	9	Scattered	.0203	.0354	.0457	.0533	.0591	.0675	.0743
20 x 20	36	Direct	.0243	.0404	.0512	.0599	.0673	.0795	.0886
	36	Scattered	.0243	.0428	.0570	.0670	.0740	.0833	.0891
20 x 20	144	Direct	.000561	.000933	.00118	.00138	.00156	.00184	.00205
	144	Scattered	.00260	.00543	.00758	.00918	.01043	.0122	.0134
20 x 40	9	Direct	.0667	.113	.142	.166	.189	.222	.248
	9	Scattered	.0[illegible]	.0312	.0409	.0453	.0519	.0570	.0618
20 x 40	36	Direct	.0218	.0369	.0476	.0555	.0621	.0730	.0815
	36	Scattered	.0211	.0380	.0498	.0570	.0624	.0698	.0759
20 x 40	144	Direct	.000504	.000854	.00374	.00126	.00146	.00169	.00188
		Scattered	.00227	.00481	.00678	.00793	.00913	.0104	.0111
20 x ∞	9	Direct	.0605	.108	.139	.156	.179	.211	.234
	9	Scattered	.0139	.0237	.0300	.0341	.0370	.0413	.0442
20 x ∞	36	Direct	.0199	.0354	.0455	.0535	.0597	.0701	.0767
	36	Scattered	.0159	.0285	.0372	.0423	.0464	.0513	.0544
20 x ∞	144	Direct	.000460	.000820	00105	.06119	.00136	.00160	.00178
	144	Scattered	.00179	.00376	.00511	.00610	.00672	.00784	.00852

TABLE 6

Engineering Manual Direct and Scattered Ground Contributions (One-Story Structure, 5 ft. Detector Height, 1.25 mev Radiation)

Building (ft.)	Wall thickness (psf)	Radiation component	W_c(ft.) 10	20	30	40	50	70	90
40 x 40	9	Direct	.0380	.0712	.0942	.0113	.131	.159	.180
	9	Scattered	.0152	.0253	.0329	.0363	.0420	.0454	.0488
40 x 40	36	Direct	.0140	.0263	.0348	.0417	.0477	.0579	.0667
	36	Scattered	.0169	.0308	.0405	.0474	.0523	.0575	.0605
40 x 40	144	Direct	.000324	.000609	.000806	.000960	.00112	.00135	.00155
	144	Scattered	.00182	.00391	.00555	.00650	.00724	.00835	.00872
80 x 80	9	Direct	.0243	.0479	.0716	.0808	.0960	.121	.141
	9	Scattered	.00887	.0143	.0183	.0205	.0229	.0254	.0270
80 x 80	36	Direct	.00796	.0157	.0235	.0265	.0316	.0397	.0491
	36	Scattered	.0102	.0170	.0223	.0258	.0281	.0314	.0331
80 x 80	144	Direct	.000207	.000409	.000611	.00069	.000823	.00104	.00121
	144	Scattered	.00111	.00225	.00309	.00358	.00410	.00476	.00505

beyond this minimum were extrapolated with the extrapolated curve becoming tangent to a constant value as W/L = 0. These extrapolated values were as much as 10 per cent less than the calculated ΔG_d value.

The NSS Compilation Program for Finite Fields of Contamination

Eisenhauer[20] has recently completed a program to compute the effect of a finite field of contamination using transmission and scattering coefficients computed by the Monte Carlo method by Berger.[15] The advantages of this type of calculation are, first, that it provides a completely different method of calculation starting with different assumptions and a different set of parameters and input data, against which the current limited strip calculation may be compared and, second, since this program utilizes transmission coefficients computed by the Monte Carlo method it may truly be thought of as a numberical representation of the actual experiment. This code has been designed to compute the dose contribution to a detector located behind a vertical wall, from contamination located in a rectangular area, called a source patch (with its axis parallel and perpendicular to the wall) through a vertical rectangular section of the wall. Detector, wall section, and source patch may be located at any arbitrary position in relation to each other. Individual contributions from each source patch representing differential areas of a field are computed and presented separately. Since the calculation is designed for finite fields of contamination, air scattering and attenuation are neglected. That this effect is negligible for finite fields of the size of interest may be quickly demonstrated. The dose rate from a limited circular field of contamination to a detector located a height h above it is:

$$D = 2\pi S_o q \int_h^{R_o} \frac{e^{-\mu\rho} B(\mu\rho)}{\rho}\, d\rho$$

where μ = total cross section for air 1/450 ft. S.T.P.

S_o = specific irradiance of the source (rads/hr curie) at 1 ft.

q = source density (curies/sq. ft.)

h = detector height (ft.)

R_o = outer slant radius of the field (ft.)

which in the absence of scattering (all collisions are assumed absorption, clearly placing an upper limit on the effect of the atmosphere) reduces to

$$D = 2\pi S_o q \left[E_1(\mu h) - E_1(\mu R_o)\right]$$

where

E_1 = the exponential integral of the first kind

if the atmosphere is totally neglected μ is zero and the corresponding equation becomes:

$$D = 2\pi S_o q \ln \frac{R_o}{h}$$

The maximum error introduced by neglecting the atmosphere would thus become

$$\text{Error} = 1 - \frac{E_1(\mu h) - E_1(\mu R_o)}{\ln \frac{R_o}{h}}$$

Field Radius (ft.) =	0	10	20	30	50	70	100
Error (%) =	0	1.2	2.2	3.0	4.3	5.5	6.8

The dose resulting from uncollided photons is computed in Eisenhauer's program by first determining if a straight line, from the center of the source patch to the detector, passes through the wall area (see Figure 21). If it does, it is assumed that all the contamination in the rectangular source patch is concentrated at the center of that patch. The dose at the detector is computed by reducing the output of that contamination by the distance to the detector squared and exponential attenuation along the slant distance through the wall (determined by the straight line connecting the source patch to the detector location). Scattered radiation is computed in a

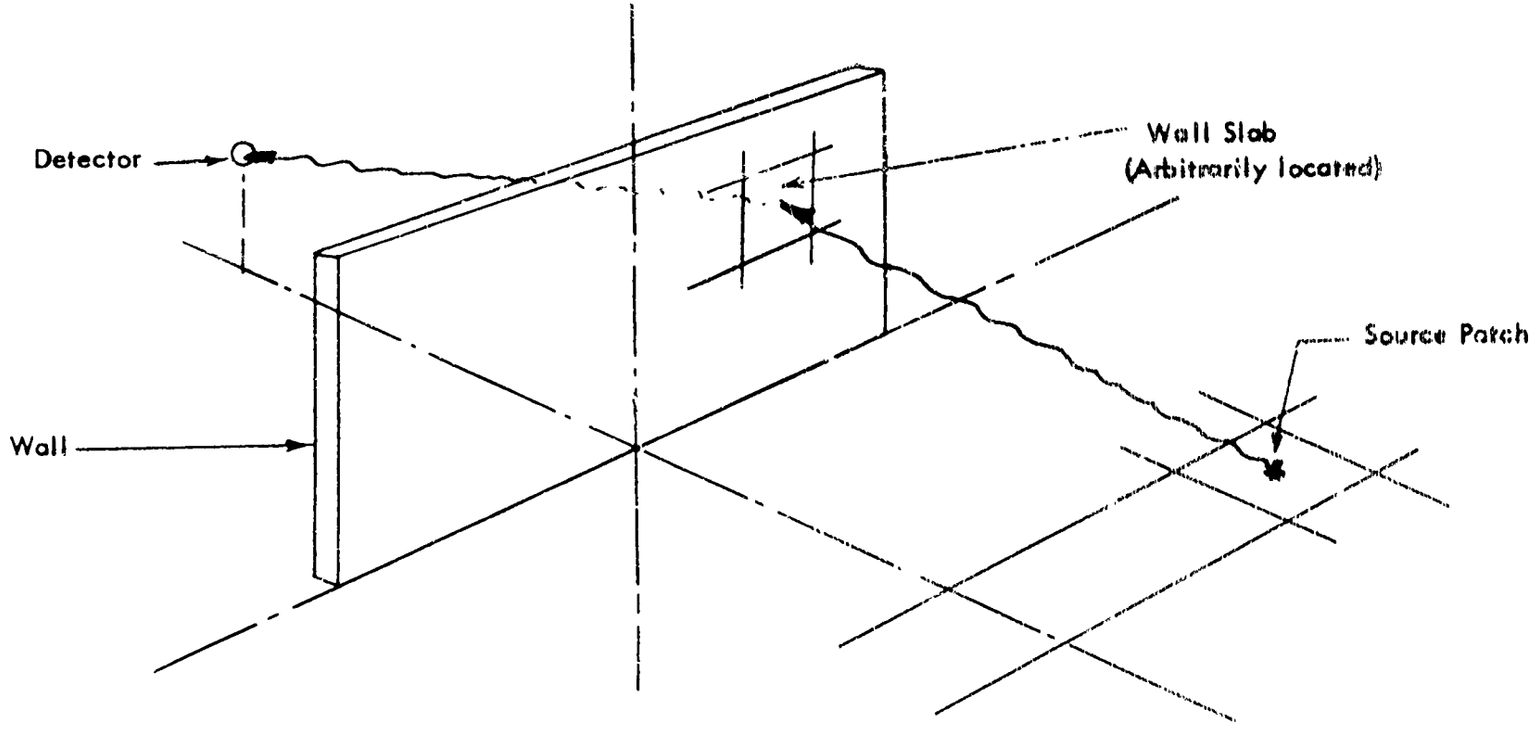

GEOMETRY FOR CALCULATION

Figure 21

of the rectangular wall area of interest and then drawing a second line from this point to the detector location. The angle made by these two lines is then determined and a transmission coefficient for scattered radiation is interpolated from the Monte Carlo transmission factors of Berger. The radiation emanating from the source patch is then reduced by the radius to the center of the wall area squared, the transmission coefficient, and the radius to the detector squared.

Clearly, both the wall and source patch grid must be chosen with care so that further reduction in grid size will yield a negligible change in results. Exploratory calculations indicate that for a detector one or more wall heights behind the wall, located at the wall mid-height, a square wall grid one-half wall height in dimension together with source patches of a similar size for the first two wall heights away from the wall and twice this size beyond, produces results that are within 1 per cent of those produced by a grid one-fourth as large. Eisenhauer[20] estimates that this program produces results which are accurate to about 5 per cent if the grid sizes are properly chosen.

After preliminary evaluation of the program the above-mentioned grid size was selected as adequate for these studies. The resultant dose contribution from a source patch on the right of the centerline through the detector perpendicular to the wall are:

1. The direct contribution — the dose contribution that proceeds directly to the detector without scattering. Since the detector is located at the wall mid-height, contribution arises through the lower half of the wall only (direct).
2. The wall-scatter contribution through a wall slab in the lower half of the wall to the right of the centerline (wall scatter lower).
3. The symmetric wall-scatter contribution through a wall slab symmetrically located on the left of the centerline (symmetric scatter lower).
4. The wall-scatter contribution through a wall slab in the upper half of the wall to the right of the centerline (wall scatter upper).
5. The symmetric wall scatter contribution through the upper wall slab symmetrically located from (4) to the left of the centerline (symmetric scatter upper).

Although the balance between direct and scattered radiation is set by the wall thickness, the division between the modes of scatter penetration seems quite general (at least for the cases investigated, between one-quarter and four mean free path thickness). For source patches located close to the wall the wall-scatter from the upper half of the wall is generally from 5 to 20 per cent of wall scatter from the lower portion. As the distance from the source patch to the wall

increases, this division becomes more nearly equal, with values generally within 10 per cent of one another at 80 ft. distance. Scattered radiation arriving through symmetrically located detectors generally behaves similarly when the source patch and wall slab are on or near the centerline. As either the slab or the source patch moves off-center, however, the symmetric scatter radiation contribution decreases more markedly. Results obtained for a 20 by 20 ft. square building with a 5 ft. detector height are illustrated in Figure 22 for each radiation component. The important feature of Figure 22 is the shape of the curves as the width of the contaminated area increases. Each component of transmitted radiation increases in almost the same way.

The NBS Monte Carlo compilation program is both extremely flexible and easy to use (though summarizing the results in a form usable for this study necessitated much manual labor in generating the required number of "numerical experiments" with which the present method of calculation could be evaluated. As an initial study, only the single detector height of 5 ft. was chosen, together with a structure wall height of 10 ft. Building size and wall thickness were then varied and the data were summarized so that the finite rectangular limited field of contamination surrounding a structure could be calculated. The data obtained from this series of calculations are summarized in Table 7.

The two methods of calculation compared

As illustrated earlier in this chapter, the maximum effect of air scatter and attenuation on the radiation originating from contaminated areas up to 100 ft. wide is only approximately 7 per cent. If both methods of calculation produce the same results, agreement should be within this 7 per cent, the engineering manual results being lower than those computed by the NBS Monte Carlo compilation method. Figures 23, 24, and 25 present this comparison for total dose as a function of width of the contaminated field. Figure 23 represents a case in which the eccentricity (W/L) of the building is varied from zero to one with all other parameters held constant. Figure 24 presents a series of calculations in which only the wall thickness is varied; Figure 25 represents two cases identical except for building plan area. These graphs indicate excellent agreement in total dose as paedicted by the two methods. The mean value of the ratio of the total dose as computed by the NBS methods to that computed by the Engineering Manual method for all cases investigated is .98 (when the ratio is computed at W_c/h = 2,3,4,6,8, 10,12, 14 for each case investigated), with average values ranging from .91 to 1.04 for any one structure design. It was expected that this ratio would be slightly greater than one (because atmospheric effects were neglected in the NBS method) rather than less than one. This minor difference probably was caused by the accuracy to which the engineering method graphs may be read. Since the ratio is so close to one and since the structure investigated was varied in size, wall thickness, and

TABLE 7

Scattered and direct contribution* as computed by the NBS Monte Carlo compilation procedure for a rectangular field of contamination surrounding the protection structure (5 ft. detector height 1.25 mev radiation)

Building (ft.)	Wall thickness (psf)	Radiation component	Field width (ft.)								
			5	10	15	20	30	40	50	60	∞
20 x 20	9	Direct	.048	.084	.114	.138	.177	.207	.232	.253	.271
	9	Scattered	.006	.012	.015	.018	.023	.026	.029	.031	.033
20 x 20	36	Direct	.020	.035	.047	.058	.074	.088	.098	.108	.115
	36	Scattered	.010	.020	.027	.033	.041	.048	.053	.057	.060
20 x 20	144	Direct	.0006	.0011	.0015	.0019	.0025	.0030	.0034	.0037	.0041
	144	Scattered	.0008	.0025	.0037	.0047	.0062	.0073	.0083	.0090	.0096
20 x 40	36	Direct	.016	.029	.039	.048	.062	.074	.083	.091	----
	36	Scattered	.008	.015	.021	.025	.032	.037	.041	.045	----
20 x ∞	36	Direct	.013	.023	.031	.037	.048	.056	.063	.069	.074
	36	Scattered	.007	.014	.019	.023	.028	.033	.036	.039	.041
40 x 40	36	Direct	.013	.023	.032	.040	.055	.066	.075	.083	----
	36	Scattered	.004	.009	.013	.016	.021	.025	.028	.030	----

*Normalized so as to make the response 3 ft. above an infinite field of contamination 1.0 if the effects of the atmosphere were included.

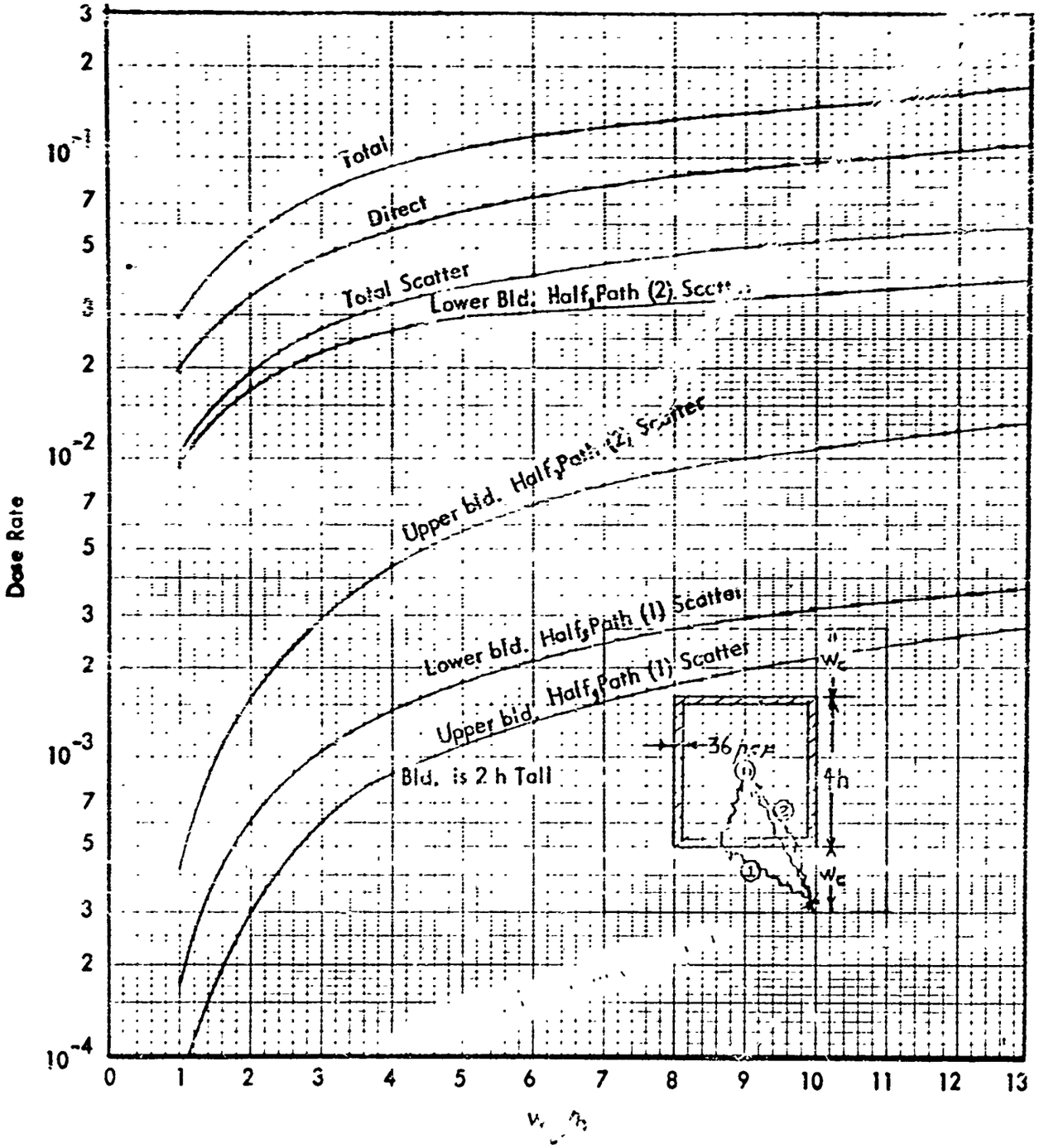

DOSE COMPONENTS IN A 20 x 20 ft BUILDING

Figure 22

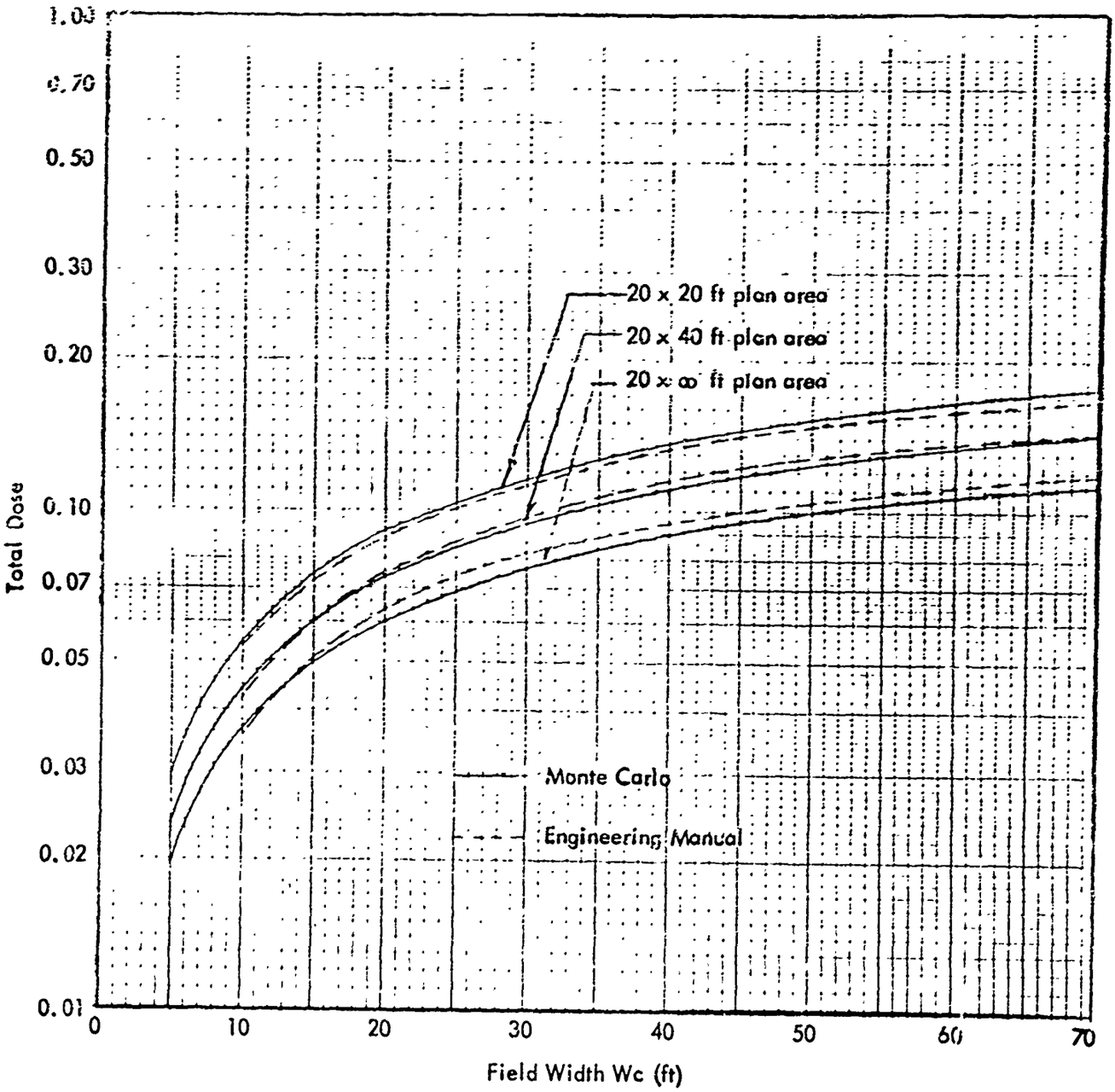

TOTAL GROUND DOSE FOR BUILDINGS OF DIFFERENT ECCENTRICITIES
(36 psf Exterior Wall 10 Feet High, Detector Height 5 Feet)

Figure 23

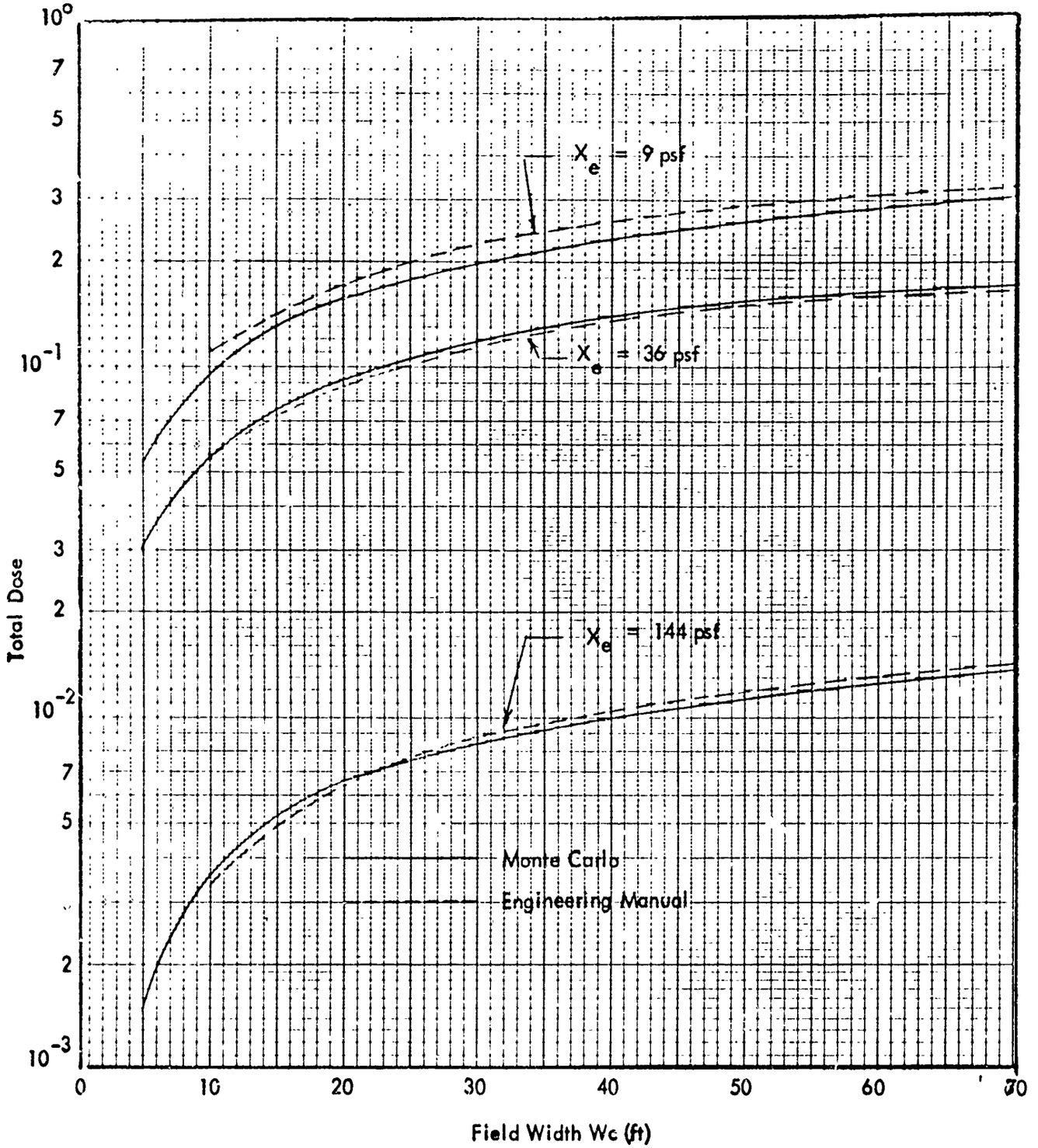

TOTAL GROUND DOSE FOR BUILDINGS OF DIFFERENT WALL THICKNESS
(20 x 20 ft Plan Area, 10 ft Wall Height, Detector Height 5 ft)

Figure 24

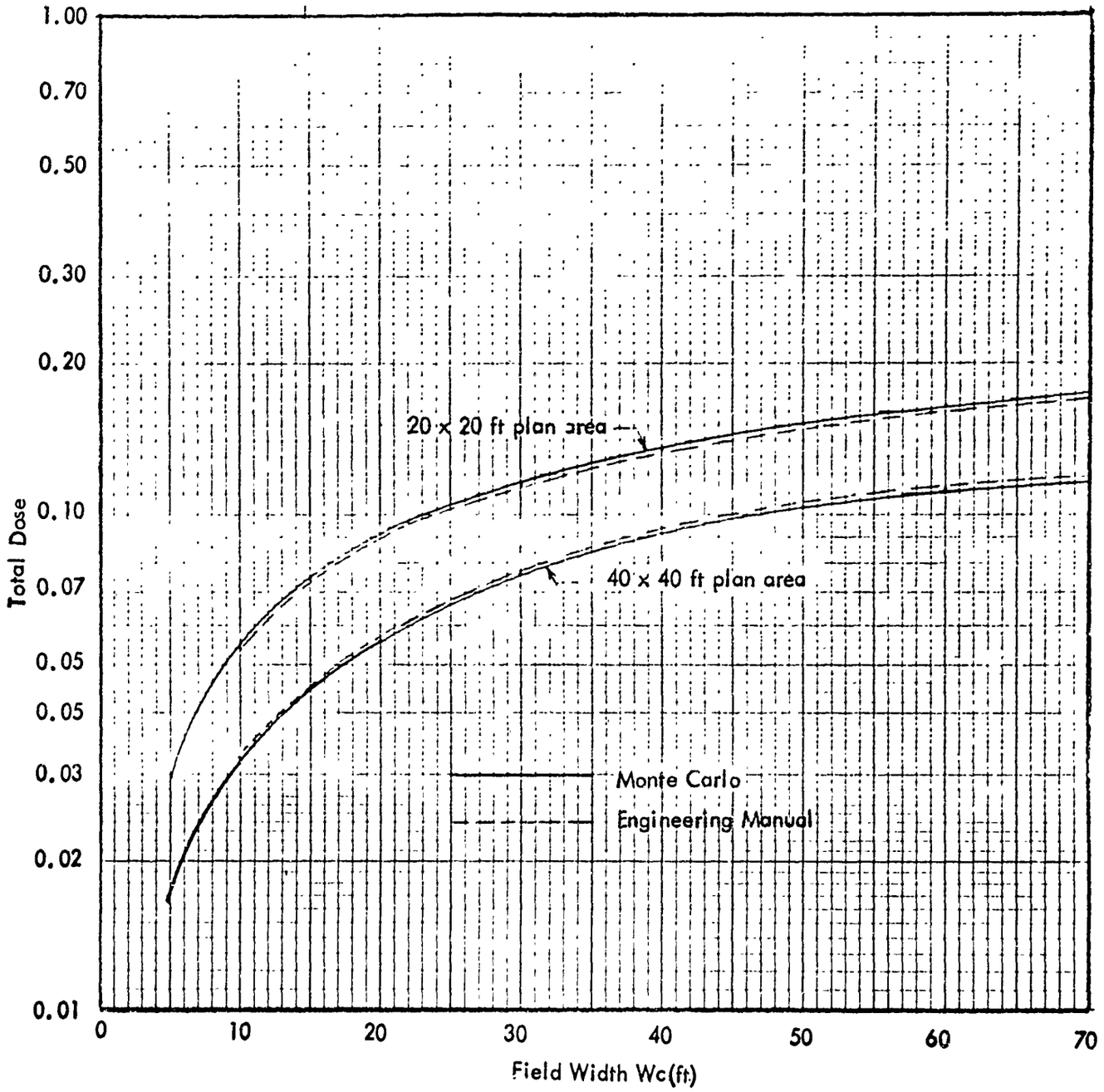

TOTAL GROUND DOSE FOR BUILDINGS OF DIFFERENT SIZE
(36 psf Exterior Wall 10 Feet High, Detector Height 5 Feet)

Figure 25

eccentricity, it may be safely concluded therefore that at first-floor locations as typified by detector height of 5 ft., the current method of computing the effect of finite rectangular fields of contamination is adequate.

Unfortunately there was not enough time to generate a similar group of data for comparison at other detector heights (for example, in basement areas and upper-floor locations) in order to make the conclusions more general. In an attempt to estimate the effects at other detector locations, the scatter and direct dose compared component by component. A surprising result was uncovered: although the ratio of either direct or scattered dose as computed by the NBS Monte Carlo Method to that computed by the engineering method was very nearly constant as a function of field size (significant variations from the mean value occurred only within the first 15 ft. of field size), this ratio varied significantly from one. Table 8 presents a summary of these data computed, as before, for each case investigated at field widths of 5, 10, 15, 20, 30, 40, 50, and 70 ft.

TABLE 8

Mean ratios of scatter and direct radiation as computed by the engineering method (10 ft. structure height, 5 ft. detector height)

			Ratios		S_w	
Parameter varied	Structure (ft.)	Wall thickness (psf)	Direct	Scat.	Old	Indicated
	20 x 20	9	1.13	.513	.178	.11
Wall thickness	20 x 20	36	1.45	.751	.475	.34
	20 x 20	144	1.92	.846	.828	.70
	20 x 20	36	1.45	.751	.475	.34
Eccentricity	20 x 40	36	1.39	.714	.475	.33
	20 x ∞	36	1.08	.800	.475	.37
	20 x 20	36	1.45	.751	.475	.34
Size	40 x 40	36	1.48	.541	.475	.27

Sizable variations between the ratio of direct and scattered radiation occur as a function of wall thickness, eccentricity, and structure size. Because data available are limited, it is difficult either to pin down the reasons for this variation

or to recommend a change. Since the ratios of total radiation computed by both methods were so nearly one, however, the ratio of scattered to total radiation, $S_w(X_e)$, used in the current methodology becomes suspect. The values of this parameter required to make the ratios of Table 8 equal to one are presented in that table and in Figure 26, together with the values currently used. Because of this discrepancy we must therefore caution that at this time the conclusion that the engineering method of computation is valid for limited fields of contamination may be made only for locations on the first floor of a structure. Other locations, where the relative importance of direct or scattered radiation is considerably different (as in basement areas or upper-floor locations where the field is shadowed by a thick floor) must be investigated further.

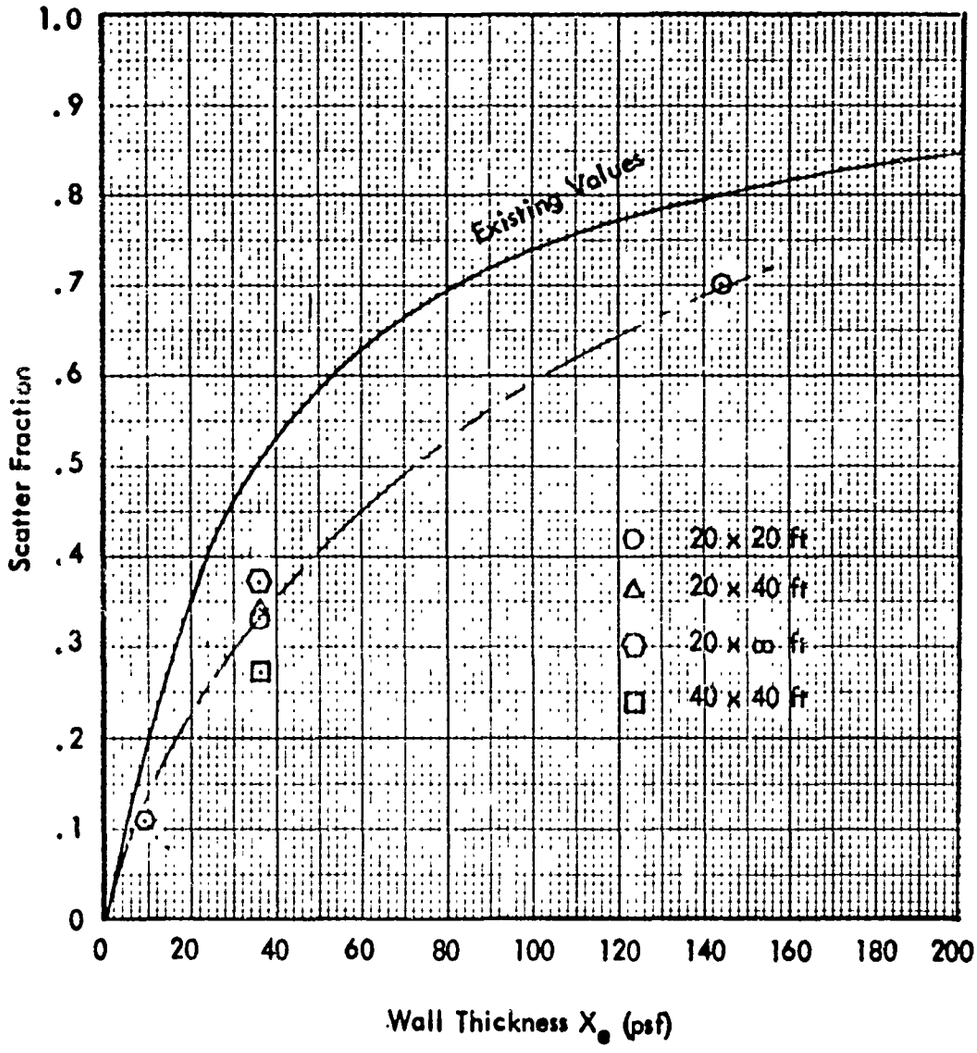

FRACTION OF TOTAL RADIATION THAT IS SCATTERED

Figure 26

CHAPTER 5

CONCLUSIONS AND RECOMMENDATIONS

In this study we have examined the new method[1] proposed for computing the attenuation of "in and down" scattered radiation and the current method of computing the effects of finite fields of contamination so that we might recommend improvements and up-dating for OCD documents OCD-TR-20, Volumes 1 and 2, "Shelter Design and Analysis."

In and Down Scattered Radiation

The new barrier factor $B'_o(X, \bar{\omega})$ computed for in and down scattered radiation, based on the assumption of Compton first collision scatter in the structure walls, has been found to provide significantly better agreement with existing experimental measurements. Comparing this factor with approximately 350 experimental measurements, we found that the new method was generally conservative, predicting dose rates from ground-based sources of contamination 18.5 per cent higher than those measured, with a standard deviation of 13.5 per cent.

It is recommended that this new barrier factor $B'_o(X, \bar{\omega})$, reduced by 18-1/2 per cent, replace the currently utilized $B'_o(X)$ to improve the accuracy of the calculation method. In Chapter 3 of this report we provide detailed recommendations on the steps required to effect this change in both the Engineering Manual, OCD TR-20, Vol. 1, and the equivalent building method, OCD-TR-20, Vol. 2.

Finite Fields of Contamination

A preliminary investigation to determine the effects of finite fields of contamination for detectors on "first-floor" locations indicates excellent agreement between total doses when calculated by the two different methods. Major variations in the scatter to direct ratio were obtained by the two methods. There is, therefore, serious doubt as to the accuracy of the recommended procedures for positions where the scatter to direct ratio is significantly different from that investigated (e.g., in basement or upper-story locations where the detector is shadowed by a heavy floor slab). It is recommended that the effects of finite fields of contamination in areas where direct radiation does not provide a major dose component be studied further in order to develop a simplified method of calculation that will be accurate in all locations.

General

The current program has reviewed most of the experimental and analytical efforts devoted to shielding from contamination in a "fallout geometry." It has become evident during this review that, in addition to the two areas of inquiry that are covered in this report, several additional areas should be investigated. These are: the ratio of scattered to direct radiation, particularly as applied to finite fields of contamination in below-ground and upper-story shelter locations; a preliminary investigation of simplified methods for computing the effects of inhomogeneous floor and wall barriers; and a preliminary study of the effects of roof wash down (or other decontamination methods) and how these effects may be simply expressed (perhaps as an additional equivalent roof thickness) in each of the present methods of calculation. The latter program is suggested so that this procedure (of decontamination) may become useful in analyzing new building construction when other slanting or design techniques cannot be used. Additional effort is required in each of these areas to ensure that the appropriate methods of analysis currently used or proposed are accurate, simple, and easily usable so that they may be included with confidence in OCD publications.

REFERENCES

1. Batter, J. F., and A. W. Starbird, The Preparation of Simplified Manuals for Shielding Analysis, June 1966 Conesco 4848-1

2. Raso, D. J., Transmission of Scattered Gamma Rays through Concrete and Iron Slabs, Technical Operations, Inc., TOB 59-13, October 1959

3. Raso, D. J., Monte Carlo Calculations on the Reflection and Transmission of Scattered Gamma Radiation, Technical Operations, Inc., TOB 61-39, May 1962

4. Eisenhauer, C., An Engineering Method for Calculating the Protection Afforded by Structures Against Fallout Radiation, NBS Monograph 76, July 1964

5. Clifford, C. E., A Study of "In-and-Down" Scattering with CS-137 Gamma Radiation, Defense Chemical Biological and Radiation Laboratories, Report No. 505, August 1966

6. Velletri, J., Private Communication, February 1966

7. Kaplan, A., Basement Radiation from an Infinite Plane Gamma Source, ANS Trans. Vol. 8, No. 1, June 1965, and oral presentation

8. Kaplan, A., Private Communication, January 1966

9. Design and Review of Structures for Protection from Fallout Gamma Radiation OCD PM100-1, February 1965

10. Schmoke, M., and Schumchyk, M., Private Communication, April 1966

References (cont'd)

11. Batter, J. F., and A. W. Starbird, Attenuation of Cobalt-60 Radiation by a Simple Structure with a Basement, Technical Operations, Inc. TOB 61- 38, 1961

12. Baron, James A., et al., Final Report of 1963 Summer Shielding Institute on Fundamental Radiation Shielding Problems, Kansc State University

13. Batter, J. F., et al., Final Report on the Effect of Limited Strips of Contamination of the Dose Rate in a Multistory Windowless Building, Technical Operations, Inc. TOB 62-58, 1962

14. Starbird, A. W., The Effect of Limited Strips of Contamination on the Dose Rate in a Multistory, Windowless Structure with 40 psf Walls and 50 psf Floor, Technical Operations, TOB 63-76, October 1963

15. Berger, J. J., and Morris, E. E., Dose and Transmission Coefficients for Cobalt-60 and Cesium-137 Gamma Rays Incident on Concrete Slabs, NBS 9071, July 1966

16. Spencer, L. V., Structure Shielding Against Fallout Radiation from Nuclear Weapons, NBS 42, June 1962

17. Parker, C. M., and Hill, E. L., A Statistical Analysis of the Influence of Phase 2 Building Characteristics on Fallout Radiation Shielding, RTI, RM 154-1 June 1964

18. Shelter Design and Analysis Equivalent Building Method, TR-20, Vol. 2, October 1964

19. McDonnell, C., et al., The Barrier Attenuation Introduced by a Vertical Wall, Protective Structures Development Center, PSDC TR-15, September 1964

20. Eisenhauer, C., Private Communication, October 1966

21. LeDoux, J. C., Commander USN, Private Communication

UNCLASSIFIED

Security Classification

DOCUMENT CONTROL DATA - R&D

(Security classification of title, body of abstract and indexing annotation must be entered when the overall report is classified)

1 ORIGINATING ACTIVITY *(Corporate author)*
Conesco Division of Flow Corporation
Watertown, Massachusetts

2a REPORT SECURITY CLASSIFICATION
Unclassified

2b GROUP

3 REPORT TITLE
THE PREPARATION OF SIMPLIFIED MANUALS FOR SHIELDING ANALYSIS

4 DESCRIPTIVE NOTES *(Type of report and inclusive dates)*
Final Report

5 AUTHOR(S) *(Last name, first name, initial)*
Starbird, Albert W.,
Batter, John F.

6. REPORT DATE	7a TOTAL NO OF PAGES	7b NO OF REFS
March 1967	78	21

8a CONTRACT OR GRANT NO.	9a ORIGINATOR'S REPORT NUMBER(S)
OCD PS-65-67	4848-2
b PROJECT NO	
c	9b OTHER REPORT NO(S) *(Any other numbers that may be assigned this report)*
d	

10 AVAILABILITY/LIMITATION NOTICES
Distribution of this document is unlimited.

11 SUPPLEMENTARY NOTES	12 SPONSORING MILITARY ACTIVITY
	Office of Civil Defense (OCD) Department of the Army - OSA Washington, D. C. 20310

13 ABSTRACT

A study was undertaken to examine present and proposed methods of calculating the attenuation afforded "in and down scattered radiation by a horizontal slab, and the effects of finite fields of contamination in order to recommend improvements and updating for OCD documents TR-20, Volumes 1 and 2, "Shelter Design and Analysis."

In this study we examined the assumptions used in computing the "in and down" attenuation factor, assessed their effect on the resulting attenuation factors, and compared the results with the latest available experimental data. Recommendations are provided as to "best value" factors and how they might be included in existing publications.

The effects of finite fields of contamination were subjected to further analysis by directly comparing the existing method of calculation with results obtained using transmission coefficients calculated by the Monte Carlo method. This comparison, though complete only for above-ground locations, indicates that further study is required before the existing method of calculation can be relied upon.

DD FORM 1 JAN 64 1473

UNCLASSIFIED

Security Classification

KEY WORDS	LINK A		LINK B		LINK C	
	ROLE	WT	ROLE	WT	ROLE	WT
1. Structure shielding from fallout gamma radiation						
2. Evaluation of structure shielding theory						
3. Radiation shielding						
4. In and down scattering						
5. Finite fields of contamination						

INSTRUCTIONS

1. ORIGINATING ACTIVITY: Enter the name and address of the contractor, subcontractor, grantee, Department of Defense activity or other organization *(corporate author)* issuing the report.

2a. REPORT SECURITY CLASSIFICATION: Enter the overall security classification of the report. Indicate whether "Restricted Data" is included. Marking is to be in accordance with appropriate security regulations.

2b. GROUP: Automatic downgrading is specified in DoD Directive 5200.10 and Armed Forces Industrial Manual. Enter the group number. Also, when applicable, show that optional markings have been used for Group 3 and Group 4 as authorized.

3. REPORT TITLE: Enter the complete report title in all capital letters. Titles in all cases should be unclassified. If a meaningful title cannot be selected without classification, show title classification in all capitals in parenthesis immediately following the title.

4. DESCRIPTIVE NOTES: If appropriate, enter the type of report, e.g., interim, progress, summary, annual, or final. Give the inclusive dates when a specific reporting period is covered.

5. AUTHOR(S): Enter the name(s) of author(s) as shown on or in the report. Enter last name, first name, middle initial. If military, show rank and branch of service. The name of the principal author is an absolute minimum requirement.

6. REPORT DATE: Enter the date of the report as day, month, year, or month, year. If more than one date appears on the report, use date of publication.

7a. TOTAL NUMBER OF PAGES: The total page count should follow normal pagination procedures, i.e., enter the number of pages containing information.

7b. NUMBER OF REFERENCES: Enter the total number of references cited in the report.

8a. CONTRACT OR GRANT NUMBER: If appropriate, enter the applicable number of the contract or grant under which the report was written.

8b, 8c, & 8d. PROJECT NUMBER: Enter the appropriate military department identification, such as project number, subproject number, system numbers, task number, etc.

9a. ORIGINATOR'S REPORT NUMBER(S): Enter the official report number by which the document will be identified and controlled by the originating activity. This number must be unique to this report.

9b. OTHER REPORT NUMBER(S): If the report has been assigned any other report numbers *(either by the originator or by the sponsor)*, also enter this number(s).

10. AVAILABILITY/LIMITATION NOTICES: Enter any limitations on further dissemination of the report, other than those imposed by security classification, using standard statements such as:

(1) "Qualified requesters may obtain copies of this report from DDC."

(2) "Foreign announcement and dissemination of this report by DDC is not authorized."

(3) "U. S. Government agencies may obtain copies of this report directly from DDC. Other qualified DDC users shall request through _____."

(4) "U. S. military agencies may obtain copies of this report directly from DDC. Other qualified users shall request through _____."

(5) "All distribution of this report is controlled. Qualified DDC users shall request through _____."

If the report has been furnished to the Office of Technical Services, Department of Commerce, for sale to the public, indicate this fact and enter the price, if known.

11. SUPPLEMENTARY NOTES: Use for additional explanatory notes.

12. SPONSORING MILITARY ACTIVITY: Enter the name of the departmental project office or laboratory sponsoring *(paying for)* the research and development. Include address.

13. ABSTRACT: Enter an abstract giving a brief and factual summary of the document indicative of the report, even though it may also appear elsewhere in the body of the technical report. If additional space is required, a continuation sheet shall be attached.

It is highly desirable that the abstract of classified reports be unclassified. Each paragraph of the abstract shall end with an indication of the military security classification of the information in the paragraph, represented as *(TS)*, *(S)*, *(C)*, or *(U)*.

There is no limitation on the length of the abstract. However, the suggested length is from 150 to 225 words.

14. KEY WORDS: Key words are technically meaningful terms or short phrases that characterize a report and may be used as index entries for cataloging the report. Key words must be selected so that no security classification is required. Identifiers, such as equipment model designation, trade name, military project code name, geographic location, may be used as key words but will be followed by an indication of technical context. The assignment of links, roles, and weights is optional.

14 KEY WORDS	LINK A		LINK B		LINK C	
	ROLE	WT	ROLE	WT	ROLE	WT
1. Structure shielding from fallout gamma radiation						
2. Evaluation of structure shielding theory						
3. Radiation shielding						
4. In and down scattering						
5. Finite fields of contamination						

INSTRUCTIONS

1. ORIGINATING ACTIVITY: Enter the name and address of the contractor, subcontractor, grantee, Department of Defense activity or other organization *(corporate author)* issuing the report.

2*a*. REPORT SECURITY CLASSIFICATION: Enter the overall security classification of the report. Indicate whether "Restricted Data" is included. Marking is to be in accordance with appropriate security regulations.

2*b*. GROUP: Automatic downgrading is specified in DoD Directive 5200.10 and Armed Forces Industrial Manual. Enter the group number. Also, when applicable, show that optional markings have been used for Group 3 and Group 4 as authorized.

3. REPORT TITLE: Enter the complete report title in all capital letters. Titles in all cases should be unclassified. If a meaningful title cannot be selected without classification, show title classification in all capitals in parenthesis immediately following the title.

4. DESCRIPTIVE NOTES: If appropriate, enter the type of report, e.g., interim, progress, summary, annual, or final. Give the inclusive dates when a specific reporting period is covered.

5. AUTHOR(S): Enter the name(s) of author(s) as shown on or in the report. Enter last name, first name, middle initial. If military, show rank and branch of service. The name of the principal author is an absolute minimum requirement.

6. REPORT DATE: Enter the date of the report as day, month, year; or month, year. If more than one date appears on the report, use date of publication.

7*a*. TOTAL NUMBER OF PAGES: The total page count should follow normal pagination procedures, i.e., enter the number of pages containing information.

7*b*. NUMBER OF REFERENCES: Enter the total number of references cited in the report.

8*a*. CONTRACT OR GRANT NUMBER: If appropriate, enter the applicable number of the contract or grant under which the report was written.

8*b*, 8*c*, & 8*d*. PROJECT NUMBER: Enter the appropriate military department identification, such as project number, subproject number, system numbers, task number, etc.

9*a*. ORIGINATOR'S REPORT NUMBER(S): Enter the official report number by which the document will be identified and controlled by the originating activity. This number must be unique to this report.

9*b*. OTHER REPORT NUMBER(S): If the report has been assigned any other report numbers *(either by the originator or by the sponsor)*, also enter this number(s).

10. AVAILABILITY/LIMITATION NOTICES: Enter any limitations on further dissemination of the report, other than those imposed by security classification, using standard statements such as:

(1) "Qualified requesters may obtain copies of this report from DDC."

(2) "Foreign announcement and dissemination of this report by DDC is not authorized."

(3) "U. S. Government agencies may obtain copies of this report directly from DDC. Other qualified DDC users shall request through _____."

(4) "U. S. military agencies may obtain copies of this report directly from DDC. Other qualified users shall request through _____."

(5) "All distribution of this report is controlled. Qualified DDC users shall request through _____."

If the report has been furnished to the Office of Technical Services, Department of Commerce, for sale to the public, indicate this fact and enter the price, if known.

11. SUPPLEMENTARY NOTES: Use for additional explanatory notes.

12. SPONSORING MILITARY ACTIVITY: Enter the name of the departmental project office or laboratory sponsoring *(paying for)* the research and development. Include address.

13. ABSTRACT: Enter an abstract giving a brief and factual summary of the document indicative of the report, even though it may also appear elsewhere in the body of the technical report. If additional space is required, a continuation sheet shall be attached.

It is highly desirable that the abstract of classified reports be unclassified. Each paragraph of the abstract shall end with an indication of the military security classification of the information in the paragraph, represented as *(TS)*, *(S)*, *(C)*, or *(U)*.

There is no limitation on the length of the abstract. However, the suggested length is from 150 to 225 words.

14. KEY WORDS: Key words are technically meaningful terms or short phrases that characterize a report and may be used as index entries for cataloging the report. Key words must be selected so that no security classification is required. Identifiers, such as equipment model designation, trade name, military project code name, geographic location, may be used as key words but will be followed by an indication of technical context. The assignment of links, rules, and weights is optional.